UNDERSTANDING THE PHYSICAL CONSTRAINTS OF SOIL STRUCTURE AND ITS INFLUENCE ON SOIL HYDRAULIC PROPERTIES

BY

Timothy Carl Bents

Submitted to the graduate degree program in Geography and the Graduate Faculty of the University of Kansas in partial fulfillment of the requirements for the degree of Master of Science

_____

Chairperson Daniel R. Hirmas

_____

William C. Johnson

_____

W. Dean Kettle

Date Defended: November 6, 2015

The Thesis Committee for Timothy C. Bents

Certifies that this is the approved version of the following thesis:

UNDERSTANDING THE PHYSICAL CONSTRAINTS OF SOIL STRUCTURE AND ITS INFLUENCE ON SOIL HYDRAULIC PROPERTIES

_____

Chairperson Daniel R. Hirmas

Date Defended: November 6, 2015

ABSTRACT

This research explores the application of multistripe laser triangulation (MLT) three-dimensional scanning to better understand soil structural constraints and predict soil hydraulic properties. Study sites for this work were located in Northeast Kansas, and split between the University of Kansas Field Station and the Kansas State Konza Prairie Biological Station. At each site, descriptions were made, soils were sampled, and profiles were scanned *in situ* using MLT. This thesis addressed two questions. First, do physical properties constrain the expression of soil structure? Particle-size distribution, organic carbon, and coefficient of linear extensibility were the physical properties examined and each appeared to constrain various aspects of soil structure. Second, can the soil hydraulic properties of field capacity, permanent wilting point, inflection point, and saturation water contents, saturated hydraulic conductivity, and effective porosity be predicted from MLT-quantified metrics of soil structure? Soils were equilibrated to a range of pressure potentials to generate water retention data for each site and hydraulic parameters were estimated from curves fitted to the data. These parameters were regressed against soil structural metrics to create structure-based pedotransfer functions for hydraulic properties. Results indicated that soil structural metrics can be used to successfully and accurately predict soil hydraulic properties.

ACKNOWLEDGEMENTS

This project would not have been possible without the help and support of many others. I would first like to thank my advisor, Dr. Daniel Hirmas, for bringing me on to this project and providing guidance as I floundered through. Many thanks are also due to Dr. Bill Johnson and Dr. Dean Kettle for serving on my committee. All were very patient as I wrote and provided invaluable feedback. I am indebted to Dennis Eck for accompanying me on the many late nights it took to scan the first soil profiles and sort through many technical difficulties. Jacque Miller, Aaron Koop, and Awesta Mohammad also provided me with much needed assistance when laser scanning for which I am grateful. I am also thankful to the Rutgers soil lab, primarily Matthew Patterson, who helped augment my data last minute. My dog, Ellie, for keeping me company for the many hours of sitting and writing, and for reminding me to go outside to enjoy the simple things. And most importantly, to my wife Alyson. I am so thankful for your late-night encouragement when I wanted to be doing anything but thesis work, your willingness to embark on this Kansas adventure with me, and your continued love and support.

TABLE OF CONTENTS

CHAPTER 1. INTRODUCTION

Soil structure, or the alignment of soil particles into repeating shapes, or peds, is a natural phenomenon common to most soils and created through a variety of processes (Hillel, 2004). While quantification of soil pores as they apply to soil structure has been addressed for decades (e.g., Baver, 1933), no one method has adequately described the nature of such pores quantitatively. Instead, semi-quantitative (Harden, 1982) to qualitative (Schoeneberger et al., 2012) methods have been relied on to understand soil structure.

Recently, a method was developed that used multistripe laser triangulation (MLT) three-dimensional scanning of a soil profile to derive metrics which describe interpedal pores from resulting scans (Eck et al., 2013). This method was able to describe the size, structural surface fracture, abundance, and orientation of those pores. My intent was to build upon this work and investigate how different properties of soil relate to soil structure.

In this thesis, my goal was to first understand what physical constraints may exist which limit or promote the formation of soil structure. There are many physical properties that are routinely measured, such as particle-size distribution, coefficient of linear extensibility, and organic carbon. In chapter 2, I examined how these properties constrain the expression of soil structure in diverse soil types.

In chapter 3, my focus turned towards understanding how soil structure impacts soil hydraulic properties. The goal for this chapter was to develop MLT-derived, structure-based pedotransfer functions. A pedotransfer function uses basic soil information to predict more difficult to measure properties. In my study, saturated hydraulic conductivity, water contents at field capacity, permanent wilting point, S-index, and saturation, and effective porosity were all

predicted using multivariate regressions. The regressions for all but effective porosity included at least one MLT metric. This thesis provides a framework for conducting additional research utilizing MLT-derived metrics of soil structure.

REFERENCES

Baver, L.D. 1933. Soil porosity as an index of structure. Soil Science Society of America Journal. 14:83-85.

Eck, D.V., D.R.. Hirmas, and D. Giménez. 2013. Quantifying soil structure from field excavation walls using multistripe laser triangulation scanning. Soil Science Society of America Journal. 77:1319-1328.

Harden, J.W. 1982. A quantitative index of soil development from field descriptions: examples from a chronosequence in central California. Geoderma. 28:1-28.

Hillel, D. 2004. Introduction to Environmental Soil Physics. Academic Press, San Diego, CA. p.73-89.

Schoeneberger, P.J., D.A. Wyocki, E.C. Benham, and Soil Survey Staff. 2012. Field book for describing and sampling soils, Version 3.0. Natural Resources Conservation Service, National Soil Survey Center, Lincoln, NE.

CHAPTER 2. DOES PARTICLE-SIZE DISTRIBUTION, SOIL ORGANIC MATTER OR COEFFICIENT OF LINEAR EXTENSIBILITY CONSTRAIN THE EXPRESSION OF SOIL STRUCTURE?

ABSTRACT

Understanding the factors that most constrain the expression of soil structure may aid in the pedogenic interpretation of a soil and provide a clearer picture of how soils develop. In this study, quantified metrics of soil structure using multistripe laser triangulation (MLT) three-dimensional scanning were compared against physical properties of particle size, soil organic carbon, and shrink swell capacity to examine how these properties constrain the expression of soil structure. Soils from the University of Kansas Field Station were sampled in this work and provided a range in soil texture, soil structure, soil organic carbon, coefficient of linear extensibility, and parent materials. Bivariate box-and-whisker bagplots were used to understand general trends in how physical factors affected soil structure. Soil structure metrics were divided into four categories based on the properties of the interpedal macropores: size, abundance, orientation, and structural surface fracturing. Size of soil structural pores was constrained by sand and clay percentages. At high clay percentages, pore sizes were large; conversely, at high sand percentages, pore sizes remained small. Abundance of soil pores was constrained by fine clay (< 2 μm) and sand percentages. Soil pores became more abundant as the fine clay percentage increased, and soil pores became scarce as sand percentage increased. Orientation of pores was constrained by depth and fine clay percentage. Structural pores became oriented more vertically, towards prismatic structure with depth. Structural surface fracture of pores was constrained by soil organic carbon and clay. Increased fracturing was observed with increasing

clay content. The physical constraints on the expression of soil structure found in this study have important pedological implications in interpreting the genesis and age of a soil.

INTRODUCTION

Soil structure —the arrangement of primary soil particles that formed from pedogenic processes and result in repeating peds— is a morphological property that controls numerous soil processes (Hillel, 2004). Soil structure controls many soil processes, including soil water flux, soil water redistribution, solute transport and soil respiration (van Genuchten, 1980; Neilsen et al., 1986; Flury et al., 1994; Ersahin et al., 2002; Cook et al., 2007). In soil water flux, the largest pores in a pore-size distribution are typically structural ones, and these macropores affect water retention of soils (Durner, 1994). In soil water redistribution and solute transport, soil structural pores become major conduits for water or dissolved solutes to move through, bypassing the soil matrix and moving through the soil profile more rapidly than in unstructured soils. Structural macropores also allow gasses to exchange more readily than in unstructured soils.

When describing soil structure in the field, categorical structure types are used to describe ped shape including granular, angular or subangular blocky, prismatic, and platy (Schoeneberger et al., 2012). Each of these structure types is also described by grade, the extent to which structure is visually expressed, and size (Schoeneberger et al., 2012). The resulting description of soil structure is informative but not easily quantifiable.

Despite the research into the importance of soil structure, a method to quantify this property has remained elusive (Young et al., 2001, Hartemink and Minasny, 2014). Recently, however, a method was developed to quantify soil macropores *in situ* using a three dimensional (3-D) scanning technique known as multistripe laser triangulation (MLT) (Eck et al., 2013). In that study, an MLT scanner was used in the field to capture interpedal soil pores from a prepared soil excavation wall.

In this work, I sought to examine if the expression of soil structure quantitatively measured by MLT scanning was constrained by soil physical properties. Previous studies have shown that physical properties such as organic carbon (Blanco-Canqui et al., 2013) and clay content (Horn et al., 1994) do, in fact, constrain soil structure. However, these studies were unable to directly quantify soil structure at the field scale. One additional property I hypothesized could directly affect soil structure was the shrink-swell capacity of a soil. Coefficient of linear extensibility (COLE) is an index used to indicate the degree to which soil will expand upon wetting and shrink upon drying (Schafer and Singer 1976). To best understand how each physical property may constrain the expression of soil structure, particle-size distribution (PSD), soil organic carbon (SOC) and shrink-swell capacity (i.e., COLE) were compared to quantified metrics of soil structural macropores.

METHODS

Site Description

The five sites used in this study were located within the University of Kansas Field Station (KUFS) and are shown in Fig.1. The KUFS is located within Jefferson, Douglas, and Leavenworth counties in northeast Kansas. Each site was chosen to represent differing landscape positions and parent materials to sample a diversity of soil structural expression and soil physical properties.

The first site was located within the Nelson Environmental Study Area (NESA). The NESA is undergoing plant succession following abandonment in 1984 from use as a hay field, and is currently being colonized by native plants from a nearby prairie (Foster, 2001). The soil

at this site was mapped as a Grundy series, (fine, smectitic, mesic, Oxyaquic Vertic Argiudoll) (Soil Survey Staff, 2015). The second site, Bluff Field, located within the Rockefeller Experimental Tract of the KUFS was a native prairie until 1948, when it was allowed to undergo forest succession (Fitch, 1965; Kettle et al., 2000). Elms (*ulaius spp*.) were the dominant trees growing at this site, though the area used in this study was recently cleared and mowed. The soil at this site was mapped as an Oska series (fine, smectitic, mesic Vertic Argiudoll) (Soil Survey Staff, 2015). The third site, Hill Field, was within the Fitch Natural History Reservation. This site was tallgrass prairie through the 1850's and was used as pasture until approximately 1948 (Fitch, 1965). Since that time, no management has occurred at this site, which has allowed early successional trees to dominate the area (Fitch, 1965; D. Kettle, personal communication, 2015). The soil at this site was mapped as a Rosendale series, (fine, mixed, superactive, mesic Typic Eutrudept) (Soil Survey Staff, 2015). The fourth site was within Management unit 1007 of the Robinson Tract. This site was historically used as a brome grass-hay field. Since 1976, the site has been managed by occasional mowing to control woody vegetation (D. Kettle, personal communication, 2015). The soil at this site was mapped as a Grinter series (mixed, mesic Lamellic Udipsamment) (Soil Survey Staff, 2015). The fifth site was located at the Native Medicinal Plant Research Garden (NMPRG). This site has been used for plant research since 2009; before that time, it was tilled under corn and soybean rotation for decades, although the site was originally tall grass prairie (K. Kindscher, personal communication, 2015). The soil at this site was mapped as a Rossville series, (fine-silty, mixed, superactive, mesic Cumulic Hapludoll) (Soil Survey Staff, 2015).

Field Sampling

At each location, a 1-meter pit was excavated and the soil profile was described following Schoeneberger et al. (2012). Detailed descriptions of each profile are provided in Table 1. Triplicate samples for bulk density determination were extracted by horizon using a soil core sampler with 3 x 5.4 cm (i.d.) brass rings (SoilMoisture Equipment Corp, Santa Barbara, CA). Additional samples by horizon were collected for PSD, SOC, and COLE determination.

MLT Scanning

After sampling, soil excavation walls were carefully straightened using trowels and soil knives to prepare them for MLT scanning. Tool artifacts left on the soil surfaces were removed using a surficial flash freeze method which peeled away a thin layer of soil, leaving the natural soil surface exposed (Hirmas, 2013).

Profiles were left to air dry for 36 hours allowing interpedal soil pores to become more visible as the surface dried following Eck et al. (2013). Once dried, tape measures were placed on each side of the cleaned soil profile to georeference the resulting digital mesh. Soil profiles were scanned using a MLT Scanner (NextEngine Desktop 3D Scanner Model 2020i, NextEngine, Inc., Santa Monica, CA) at night to eliminate interferences associated with ambient light (Eck et al., 2013). The scanner was positioned approximately 43 cm from the excavation walls during scanning, as recommended by the manufacturer. Full details on scanning procedures are given in Eck et al. (2013).

The resulting data were processed in ScanStudio (NextEngine Inc., Santa Monica, CA) to align and georeferenced the scans. Interpedal pores were digitized into 2-D images following

Eck et al. (2013) and quantified using ImageJ (Research Services Branch, National Institute of Health, Bethesda, MD).

Laboratory Analyses

Particle-size distribution was determined using the pipette method (Gee and Or, 2002) on samples that were pretreated to remove organic matter. Soil organic carbon was measured as the difference between total carbon and inorganic carbon content determined by coulometry (Jackson and Roof, 1992; Engleman et al., 1985). Bulk density was determined in triplicate from sampled cores following Grossman and Reinsch (2002). Results from these tests are shown in Table 1.

As a measure of the shrink-swell capability of soils used in this study, coefficient of linear extensibility (COLE) was determined in triplicate for each sample following the $COLE_{rod}$ method developed by Schafer and Singer (1976). Briefly, samples were mixed to just below a saturated paste, left to equilibrate for 24 hours, loaded into a modified syringe which produced rods ranging from 6 to 10 cm in length. The rods were air dried and re-measured, and adjusted through an empirically derived equation following Schafer and Singer (1976) to obtain COLE values (Table 1). Statistical analyses were conducted using R (R 2.15.1) and SPSS (IBM SPSS 21).

RESULTS AND DISCUSSION

Bagplots were used in this work to understand the relationship between soil physical properties and MLT-quantified structure metrics. A bagplot is a bivariate generalization of a traditional box-and-whiskers plot (Rousseeuw et al., 1999). This type of plot shows general trends of the data and constraints can be identified visually. I interpreted the areas in the plot

outside the bag (i.e., areas without data points) to represent a constraint of a soil physical property on structural expression. Metrics resulting from MLT were divided into four categories: structural pore size, structural surface fracture, structural pore abundance, and orientation of structural pores.

Structural Pore Size

Two metrics for size were used to investigate relationships between soil structural expression and soil physical properties: feret diameter and minimum feret diameter. Feret diameter is a caliper measurement of the maximum diameter of a pore (Fig. 2). Minimum feret diameter is the caliper distance of the minimum diameter of a pore (Fig. 2).

Minimum feret diameter can be interpreted as the average width of a pore. The width of soil pores is positively related to the water holding capacity and transmissivity of the pores of a given sample (Lin et al., 1997). Both sand and clay showed strong relationships with the minimum feret of each sample (Fig. 3A-B). Sand and clay had opposite effects on the size of pores. As clay percentage increased, larger minimum feret diameters (i.e., pores of greater width), were observed. By contrast, as sand increased, the pore size decreased. This is likely due to the clay causing more cohesion between particles than with sandier soils (Kemper and Koch, 1966). The cohesive nature of clay allows for soil peds to take shape, whereas sandy soils do not tend to form structural units and instead stay in an unconsolidated single-grained state (Schaetzl and Anderson, 2005; Utomo and Dexter, 1981). In Fig. 3B, the area below the plot indicates that clay is constraining the width of soil pores to progressively become larger as the clay percentage increases.

The second size metric used was feret diameter. This metric gives an average pore length for each sample (Fig. 2). The longer the average pore length, the more interconnected pores tend

to be. That is, in a well-structured soil, the pore lengths (or feret diameters) were orders of magnitude longer than in poorly-structured soils. Sand showed a negative relationship with feret diameter (Fig. 3C) indicating that with a higher percentage of sand, elongated structural pores are less likely to develop. Clay, however, showed a positive relationship with increasing average feret diameter. Perhaps more interesting is the lack of points in the upper left corner of the plot at the lower clay percentages (Fig. 3D). The lack of data in this corner indicates that the amount of clay is constraining soil structural development. At lower clay percentages, soil structure is not well expressed, because it cannot form without added cohesion gained from increased clay percentages (Kemper et al., 1987).

Structural Surface Fracturing

Structural surface fracturing, or the perimeter of the pores divided by the area of the entire image used to represent a soil horizon, can also be interpreted as the relative surface area of the pores in a given horizon (Eck et al., 2013). With an increase in fracturing, a higher amount of structural formation is present. Particle-size distribution as well as SOC were the two factors which showed the strongest relationship with the structural surface fracture (Fig. 4). As the percent of SOC increased, so did the relative fracture surface (Fig. 4A). The highest SOC values were typically in the upper horizons with granular structure. In the topsoil, granular patterns are more common and there are many voids between granules, resulting in greater surface fracturing.

As clay percentage increased, structural surface fracturing increased as well (Fig. 4B). From approximately 30-40% clay and higher, there is a lack of observations in the lower right of the plot, which shows the constraint clay content has on structural formation. As clay content

increases, it becomes increasingly unlikely for soil not to fracture. However, when clay content was lower, samples with high relative surface fracturing typically fell in an A horizon or in one with a relatively high amount of SOC. Soil organic matter does have an effect on structural surface fracturing (Fig. 4A). To isolate the effect of clay content, B horizons were compared to the structural surface fracturing of each sample (Fig. 4C). There is a much stronger relationship between the percent clay and the structural surface fracturing when such a comparison was considered. The constraints are much more pronounced and area clearly visible on the upper left and lower right dearths of the plot. At lower percentages of clay, fracturing is limited, likely due to a lack of cohesion needed for soil structure to occur (Kemper and Rosenau, 1984). At higher clay percentages, it is difficult for structure not to form, likely due to the aggregative properties of clay into soil structure (Bronick and Lal, 2005).

Structural Pore Abundance

Soil horizons that contained well graded soil structure also had higher pore densities. Pore density is the total number of pores in a horizon divided by the area of that entire horizon. Pore density increases with increasing clay percentage; this can be seen in the bagplot of the fine clay fraction and pore density (Fig. 5A). The fine clay fraction is generally the most active portion of the clay fraction, containing minerals such as smectite (Coulombe et al., 1996). As the fine clay percentage increases, so does the pore density, indicating that more soil structure is present. The lack of observations in the upper left of this plot indicates that a sample without very much fine clay cannot easily increase in pore density. There is also a small area without observations in the bottom left of the plot where the fine clay fraction begins to reach 30-50% of

the total particle-size distribution. Within this area, the implication is that in the presence of high fine clay percentage, it is difficult for the soil not to contain macropores.

An inverse relationship was observed between sand content and pore density (Fig 5B). As the amount of sand increases, the possibility for soil structure decreases. The particles of sand are large enough that liquid will infiltrate between soil particles without the presence of macropores; the soil is not cohesive or expansive enough at high percentages of sand to form and hold in a repeated pattern of structure (Mullins and Panayiotopoulos, 1984). The lack of data in the upper right hand corner of the plot indicates that as the percent sand increases, the possibility of structure occurring and producing pore density decreases and ultimately becomes nearly impossible. A single-grain designation is used when sand dominates the profile and soil structure has not formed due to a lack of cohesion from clay (Ingles, 1962).

Orientation of Structural Pores

The orientation of structural pores was affected by the depth of the soil as well as the fine clay fraction of each sample (Fig. 6). The major ellipse angle is defined as the angle of the major axis of an ellipse drawn around a pore (Fig. 2). This measurement gives an indication of the general trend of macropores from a given soil. The orientation, ranging from 0° (horizontal) to 90° (vertical), was calculated for each macropore. These values were then averaged by horizon to return the representative orientation of each sample. The midpoint depth and the fine clay fraction showed a strong correlation with structural pore orientation (Fig. 6). In the midpoint depth plot (Fig. 6A), this trend was clearer when considering soil horizons within the upper 50 cm (Fig. 6B). If the structural pores had a combination of vertical and horizontal orientations (e.g., blocky or granular structure), the averaged major ellipse angle would be closer to 45°.

When considering the first 50 cm, the angle of structural pores increased from approximately 45° to about 60° with depth. This would indicate a higher presence of prismatic structure. Below 50 cm some profiles exhibited prismatic structure (i.e., NMPRG), the Robinson Tract had horizontally oriented clay lamellae bands, and the structure at NESA became primarily wedge shaped (Table 1). These structures create pores that vary in primary orientation angles. The varied characteristics in the deeper horizons indicate how soils developed and what pedogenic processes have taken place (Norman, 1955).

The fine clay fraction (< 2 μm) also appears to have an effect on how structural pores are oriented (Fig. 6C). The tendency appears to be that as the amount of fine clay increases, the average ellipse angle approaches 45°. This would indicate that as fine clay increases, the pores become arranged in a manner that reflects blocky structure. As the amount of fine clay lessens, the pores became more vertically oriented.

Soil Structural Constraints

Idealized plots of soil structure formation are shown in Fig. 7. Each plot represents a structural expression constrained by the physical properties investigated in this study. Fig. 7 shows that as clay content increases pore size increases as well. Beyond 40% clay content, it becomes difficult for small pores sizes to exist due to the inherent cohesiveness of clay. Additionally, at low clay contents, it becomes unlikely for larger structural pores to form.

In Fig. 7, sand is shown to constrain the number of structural macropores which can form. Sandy textures decrease soil cohesion. As sand percentages increase, the probability that structural pores will form decreases. There is also a constraint on soil structure at low sand percentages. Here, soil fines, (i.e., clay and silt) dominate the PSD, increasing the probability of

structural pore formation. The orientation of pores is constrained by the depth of soil. In this study, structural pores became more vertically aligned with depth because prismatic structure became the dominant structure type (Fig. 7).

The final constraint determined in this work was with the clay fraction unaltered by SOC (i.e., the B horizons) and the relative surface fracturing of soils (Fig. 7). Structural surface fracturing increased as clay content increased, reiterating the importance of clay content to the development of soil structure.

CONCLUSION

This work has shown that certain soil properties do limit the extent to which soil structure is expressed and if soil structure can form at all. The factors that most constrained the extent of soil structure were clay and sand percentages. Depth of the soil also had a role, but only when considering the orientation of soil pores.

Soil texture had the largest role in limiting the expression of soil structure. Sandy soils had little structural expression and structure became more prevalent as clay percentage increased. Additionally, soils with very high clay contents were always structured and pores were expressed to a high extent and formation under high clay percentages appeared to be inevitable.

Physical constraints exist that seem to limit the development of soil structure. In general, orientation is most influenced by the depth of soil, size is limited by the clay and sand content, shape is influenced by sand, clay and organic matter, and abundance is most influenced by fine clay and sand.

REFERENCES

Blake, G.R., and R.D. Gilman. 1970. Thixotropic changes with ageing of synthetic aggregates. Soil Science Society of America Proceedings. 34:561-564.

Blanco-Canqui, H., C.A. Shapiro, C.S. Wortmann, R.A. Drijber, M. Mamo, T.M. Shaver, and R.B. Ferguson. 2013. Soil organic carbon: the value to soil properties. Journal of Soil and Water Conservation. 68:129A-134A.

Bronick, C.J., and R. Lal. 2005. Soil structure and management: a review. Geoderma. 124:3-22.

Coulombe, C.E., J.B. Dixon, L.P. Wilding. 1996. Mineralogy and chemistry of vertisols. Developments in Soil Science. 24:115-200.

Durner, W. 1994. Hydraulic conductivity estimation for soils with heterogeneous pore structure. Water Resource Research. 30:211-223.

Eck, D.V., D.R.. Hirmas, and D. Giménez. 2013. Quantifying soil structure from field excavation walls using multistripe laser triangulation scanning. Soil Science Society of America Journal. 77:1319-1328.

Engleman, E.E., L.L. Jackson, and D.R. Norton. 1985. Determination of carbonate carbon in geological materials by coulometric titration. Chemical Geology. 53:125-128.

Ersahin, M.S., R.I. Papendick, J.L. Smith, C.K. Keller, and V.S. Manoranjan. 2002. Macropore transport of bromide as influenced by soil structure differences. Geoderma. 108:207-223.

Foster, B.L. 2001. Constrains on colonization and species richness along a grassland productivity gradient: the role propagule available. Ecology Letters. 4:530-535.

Fitch, H.S. 1965. The University of Kansas Natural History Reservation in 1965. University of Kansas Museum of Natural History Miscellaneous Publication. 42. Lawrence, KS.

Flury, M., H. Flühler, W.A. Jury, and J. Leuenberger. 1994. Susceptibility of soils to preferential flow of water: a field study. Water Resources Research. 30:1945-1954.

Gee, G.W., and D. Or. 2002. Particle-size analysis. In J.H. Dane and G.C. Topp (Eds.) Methods of Soil Analysis Part 4, Physical Methods. Soil Science Society of America, Madison, WI. p.255-293.

Grossman, R.B. and T.G. Reinsch. 2002. Bulk density and linear extensibility. In J.H. Dane and G.C. Topp (Eds.) Methods of Soil Analysis Part 4, Physical Methods. Soil Science Society of America, Madison, WI. p.201-228.

Hartemink, A.E., and B. Minasny. 2014. Towards digital soil morphometrics. Geoderma. 230-231:305-317.

Hillel, D. 2004. Introduction to Environmental Soil Physics. Academic Press, San Diego, CA. p.73-89.

Hirmas, D.R. 2013. A simple method for removing artifacts from moist fine-textured soils faces. Soil Science Society of America Journal. 77:591-593.

Horn, R., H. Taubner, M. Wuttke, and T. Baumgartl. 1994. Soil physical properties related to soil structure. Soil and Tillage Research. 30:187-216.

Ingles, O.G. 1962. A theory of tensile strength for stabilized and naturally coherent soils. Australian Road Research Board Procedings. 1:1025-1047.

Jackson, L.L. and S.R. Roof. 1992. Determination of the forms of carbon in geologic materials. Geostandards Newsletter. 16:317-323.

Kemper, W.D., and E.J. Koch. 1966. Aggregate stability of soils from western U.S. and Canada. USDA Technical Bulletin 1335. U.S. Government Printing Office, Washington, D.C.

Kemper, W.D., and R.C. Rosenau. 1984. Soil cohesion as affected by time and water content. Soil Science Society of America Journal. 8:1001-1006.

Kemper, W.D., R.C. Rosenau, A.R. Dexter. 1987. Cohesion development in disrupted soils as affected by clay content and organic matter content and temperature. Soil Science Society of America Journal. 51:860-866.

Kettle, W.D., P.M. Rich, K. Kindscher, G.L. Pittman, and P. Fu. 2000. A 40-year study in the prairie-forest ecotone. Restoration Ecology. 8:307-317.

Lin, H.S., K.J. McInnes, L.P. Wilding, and C.T. Hallmark. 1997. Low tension water flow in structured soils. Canadian Journal of Soil Science. 77:649-654.

Mullins, C.E., and K.P. Panayiotopoulos. 1984. The strength of unsaturated mixtures of sand and kaolin and the concept of effective stress. European Journal of Soil Science. 35:459-468.

Nielsen, D.R., M.Th. van Genuchten, and J.W. Biggar. 1986. Water flow and solute transport processes in the unsaturated zone. Water Resources Research. 22:89S-109S.

Norman, A.G. 1955. Advances in agronomy volume 7. Academic Press inc. New York, New York. p.2-35.

Rousseeuw, P.J., I. Ruts, and J.W. Tukey. 1999. The bagplot: a bivariate boxplot. Statistical Computing and Graphics. 53:382-387.

Schaetzl, R.J., and S. Anderson. 2005. Soils: Genesis and Geomorphology. Cambridge University Press, New York, NY. P.9-22 & 83-92.

Schaetzl, R., and Thompson, M.L. 2015. Soils: Genesis and Geomorphology, Second Edition. Cambridge University Press, New York, NY. p.18-20.

Schafer, W.M. and M.J. Singer. 1976. A new method of measuring shrink-swell potential using soil pastes. Soil Science Society of America Journal. 40:805-806.

Schoeneberger, P.J., D.A. Wyocki, E.C. Benham, and Soil Survey Staff. 2012. Field book for describing and sampling soils, Version 3.0. Natural Resources Conservation Service, National Soil Survey Center, Lincoln, NE.

Soil Survey Staff, Natural Resources Conservation Service, United States Department of Agriculture. Official Soil Series Descriptions. Available online. Accessed [4/25/2015].

Utumo, W.H. and A.R. Dexter. 1981. Soil friability. Journal of Soil Science. 32:203-213.

van Genuchten, M.Th. 1980. A closed-form equation for predicting the hydraulic conductivity of unsaturated soils. Soil Science Society of America Journal. 44:892-898.

Young, I.M., J.W. Crawford, and C. Rappoldt. 2001. New methods and models for characterizing structural heterogeneity of soil. Soil and Tillage Research. 61:33-45.

Table 1. Selected properties of each soil pedon used in study. See Fig. 1 for the distribution of these sites.

Horizon	Depth	Bndy†	Bulk Density	Moist color	Structure‡	PSD§			OC#	COLE††
						Sand	Silt	Clay		
	cm		g cm^{-3}			%				
				NESA (39.05696° N, 95.19058° W)						
Ap	0-8	cs	1.06±0.01	10YR 3/1	1mpl,1f,2mgr	5.1	72.6	22.3	2.82	0.043±0.01
Ap	8-22	vw	1.31±0.03	10YR 3/1	3m,cosbk, 2f,mabk	4.6	70.7	24.8	1.59	0.035±0.00
Bt1	22-39	cw	1.3±0.05	10YR 4/3	3vf,1m,co sbk, 3vfabk	4.9	65.3	29.9	0.94	0.049±0.00
Bt2	39-54	cw	1.43±0.03	10YR 4/3	1f,mpr/2f,mabk	4.8	59.1	36.1	0.62	0.069±0.02
Btss1	54-61	aw	1.44±0.01	10YR 4/4	1f pr/2vf,f abk	3.5	46.9	49.6	0.38	0.082±0.02
2Btss2	61-85	cw	1.35±0.08	10YR 5/3	3vf,f,m,2coweg	3.0	43.1	53.9	0.31	0.079±0.02
2Btss3	85-108	-	1.31±0.02	10YR 5/4	2vf,f,mweg	3.1	39.6	57.3	0.18	0.094±0.02
				Bluff Field (39.04409°N, 95.20508°W)						
A	0-5	as	0.97±0.03	10YR 3/2	2m,cogr, 1,2 msbk, 1mpl	4.5	69.5	26.0	3.91	0.052±0.01
AB	5-20	as	1.24±0.24	10YR 2/2	2m pr/ 2m-co sbk	4.6	62.7	32.7	1.62	0.080±0.02
Bt1	20-30	gs	1.13±0.04	10YR 3/3	2m pr/ 2f-m abk	3.4	45.5	51.2	1.38	0.12±0.02
Bt2	30-56	cs	1.24±0.14	10YR 3/4	3m-vc pr/3f-co abk	4.9	49.3	45.8	0.97	0.106±0.01
Bt3	56-76	cs	1.51±0.11	10YR 3/6	1mpr/3m-co abk	5.8	52.4	41.8	0.36	0.099±0.01
Bt4	76-102	vw	1.46±0.23	10YR 3/6	3co-vc abk/2mabk	7.2	51.4	41.3	0.26	0.105±0.02
				Hill Field (39.04175° N, 95.204389° W)						
A1	0-13	aw	1.08±0.08	10YR 2/1	2mgr	5.8	48.7	45.5	5.76	0.091±0.02
A2	13-28	aw	1.34±0.17	10YR 2/1	2vfsbk	6.9	34.8	58.3	4.49	0.09±0.01
Bt1	28-43	cw	1.30±0.08	10YR 2/2	2fsbk	8.2	42.6	49.2	3.39	0.103±0.00
Bt2	43-76	aw	1.14±0.14	10YR 2/2	2msbk	8.1	35.2	56.7	2.39	0.101±0.00
2Bt3	76-101	cw	1.03±0.04	10YR 4/2	1msbk	7.4	37.3	55.3	0.18	0.083±0.02
2Btk	101-121	cw	1.23±0.11	2.5Y 5/3	1msbk	5.8	51.9	42.3	< 0.001	0.073±0.02
				Robinson Tract (39.02118° N 95.20813° W)						
Ap	0-8	as	1.06±0.12	10YR 2/2	2f,m sbk/ 2m, co gr	89.9	4.3	5.8	1.84	0.012±0.00
A	8-30	vi	1.31±0.03	10YR 3/2	1m,co sbk	80.6	14.8	4.6	0.56	0.012±0.00
E1	30-42	vi	1.32±0.03	10YR 4/3	1msbk	85.0	12.1	2.9	0.15	0.012±0.00
E2	42-69	gw	1.45±0.05	10YR 5/4	1msbk	77.9	17.2	4.9	0.12	0.012±0.00
Bt1‡‡	69-107	as	1.65±0.15	10YR 5/3 (75%) 10YR 4/6 (25%)	2vc,co,m,f pr/2f, m abk	52.0	27.2	20.8	0.26	0.023±0.01
Bt2‡‡	107-122	-	1.65±0.03	10YR 4/2 (80%) 7.5YR 4/6 (20%)	2m,co abk	40.9	27.2	31.9	0.23	0.062±0.01
				NMPRG (39.00980° N, 95.206740° W)						
Ap	0-8	cs	1.03±0.01	10YR 2/1	3cogr, 2f,m sbk	17.2	60.4	22.5	1.39	0.017±0.01
A	8-20	as	1.09±0.07	10YR 2/2	1m,co pr	16.2	64.6	19.2	0.98	0.036±0.01
AB	20-33	aw	1.12±0.04	10YR 2/2	2mpr	11.0	63.4	25.5	1.18	0.042±0.02
Bt1	33-67	gw	1.08±0.07	10YR 2/2	3copr	10.5	61.5	27.9	1.18	0.040±0.01
Bt2	67-101	aw	1.13±0.03	2.5Y 3/2	3co,vc pr	12.6	63.6	23.8	0.87	0.021±0.00
Bt3	101-115	cw	1.10±0.03	2.5Y 5/3	2copr	19.2	63.2	17.6	0.36	0.020±0.00

† Bndy, Boundary; v, very abrupt; a, abrupt; c, clear; g, gradual; s, smooth; w, wavy; i, irregular.

‡ 1, weak; 2, moderate; 3, strong; vf, very fine; f, fine; m, medium; co, coarse; vc, very coarse; gr, granular; sbk, subangular blocky; abk, angular blocky; pr, prismatic; weg, wedge; /, parting to.

§ PSD, particle-size distribution.

OC, soil organic carbon.

†† COLE, coefficient of linear extensibility.

‡‡ Contained clay lamelle.

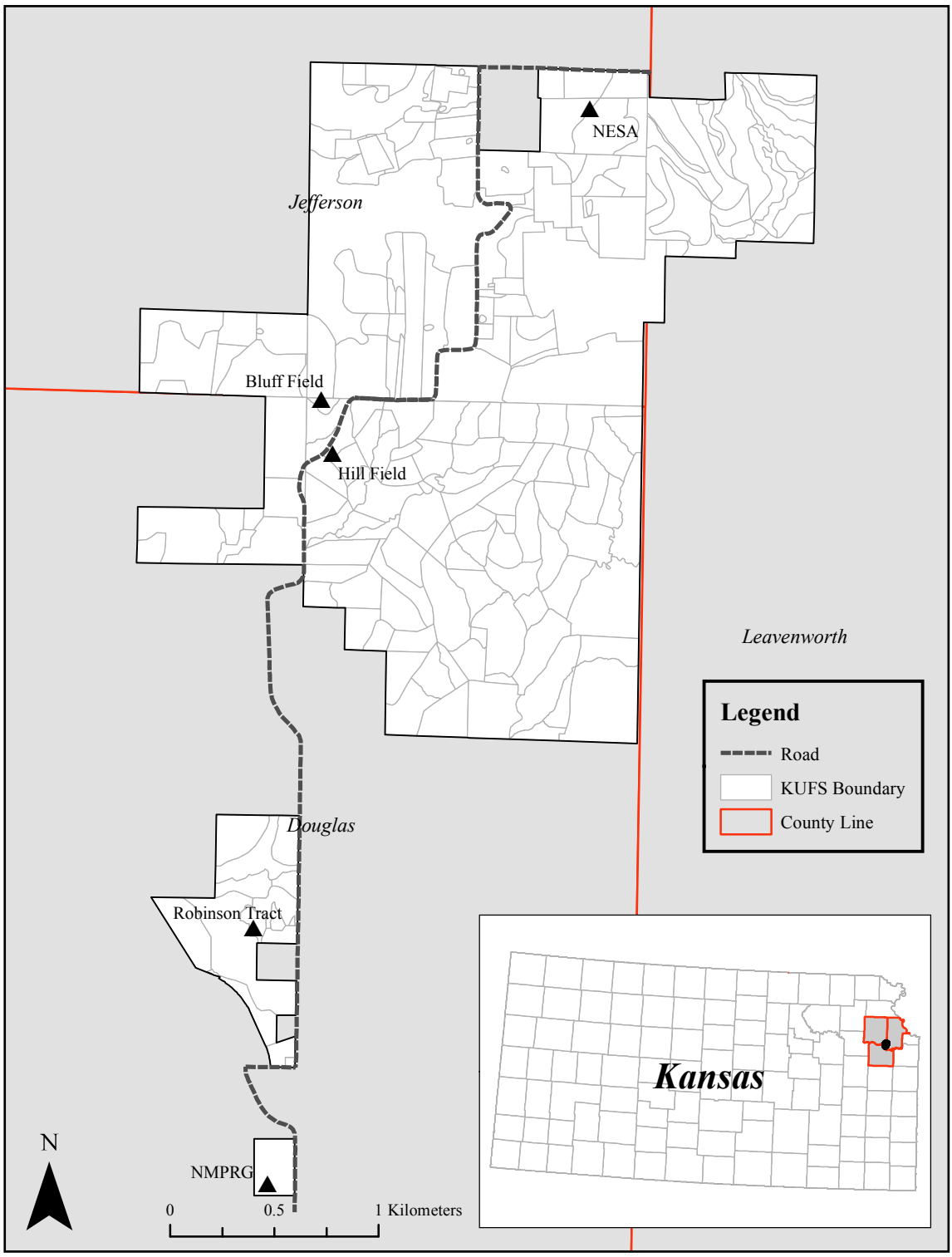

Fig.1. Distribution of sites used in this study with the boundaries of the University of Kansas Field Station (KUFS).

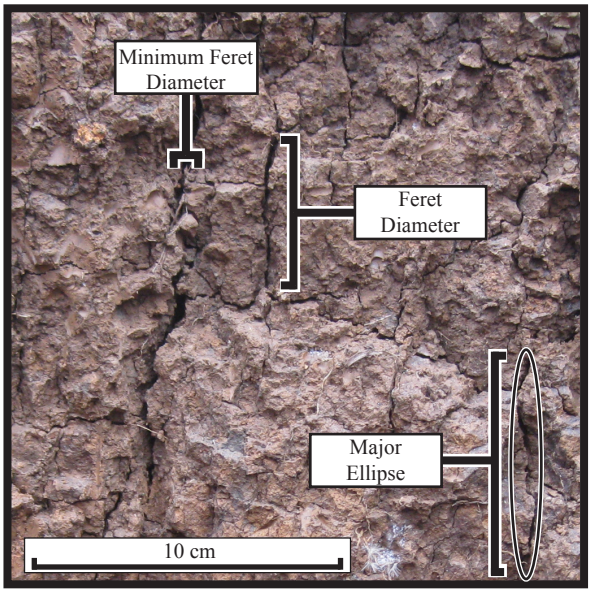

Fig. 2. Idealized macropore size measurements used in this study. Minimum feret is the shortest caliper length of a pore, feret diameter is the longest. Major ellipse is the longest axis of an ellipse drawn around a pore. Photograph is of an excavation wall at the Bt2 horizon of the Bluff Field site.

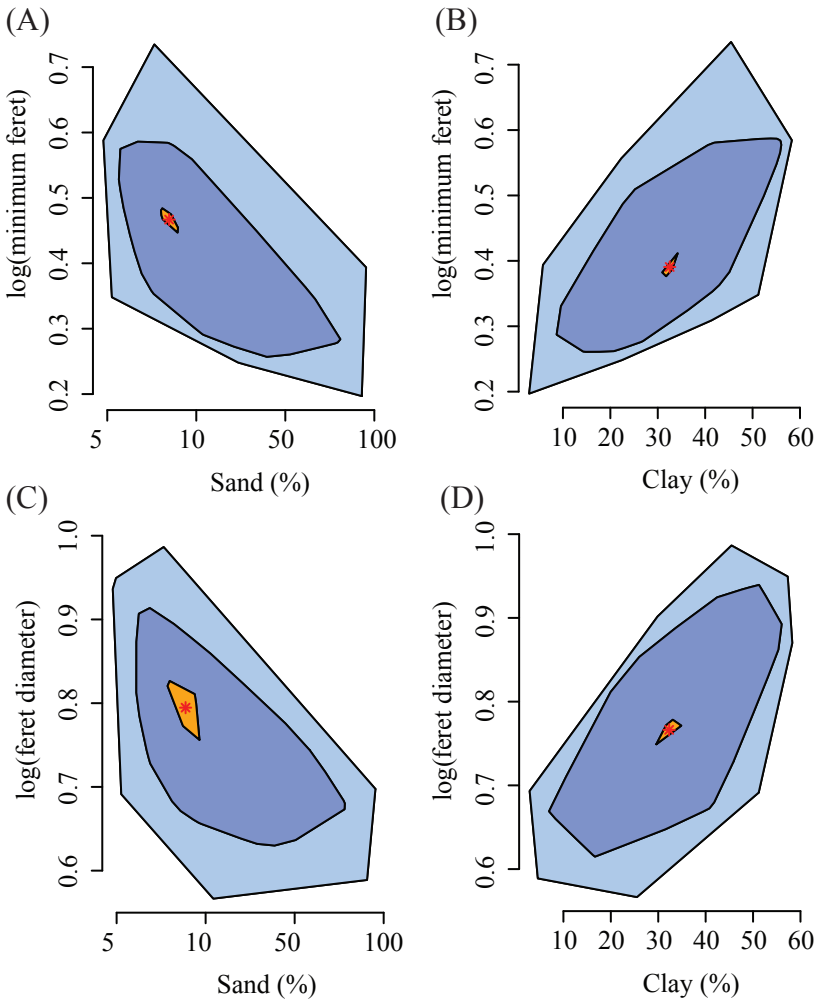

Fig. 3. Bagplots of size metrics to particle-size values of sand and clay percentages.

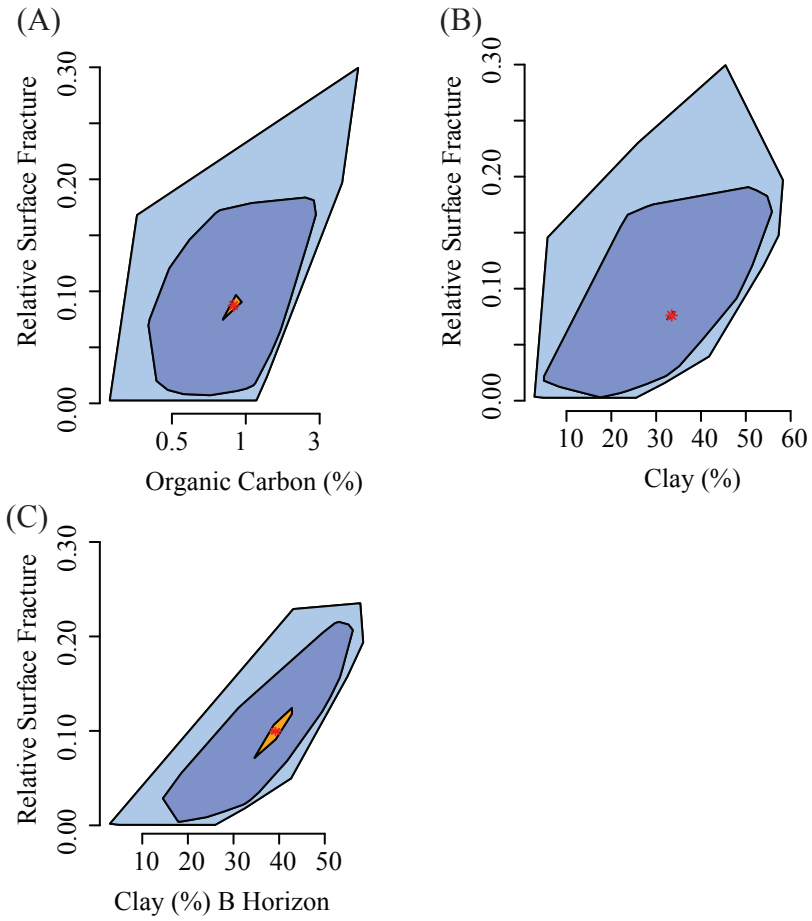

Fig. 4. Bagplots of structural surface fracturing to organic carbon and clay percentages.

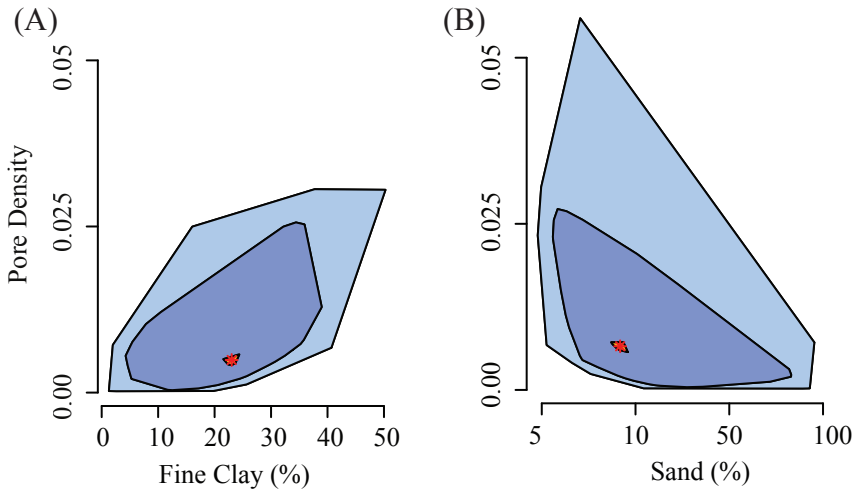

Fig. 5. Bagplots of abundance metrics to particle-size values of fine clay and sand.

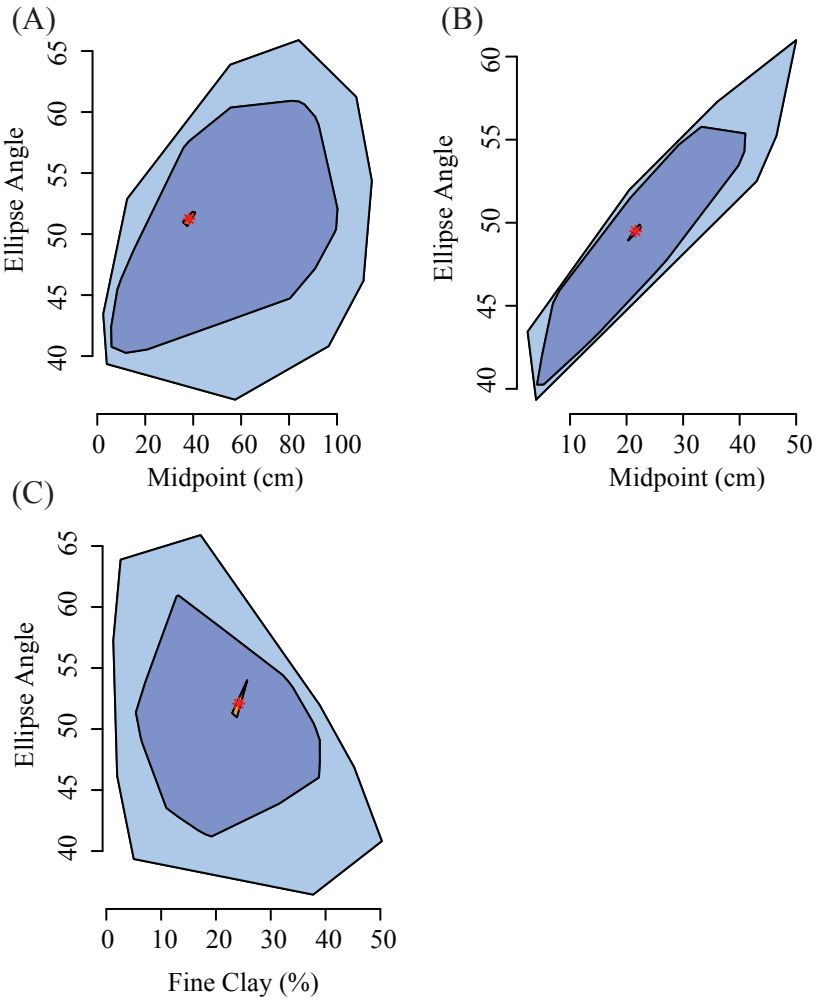

Fig. 6. Bagplots of orientation metrics to midpoint depth and fine clay percentage.

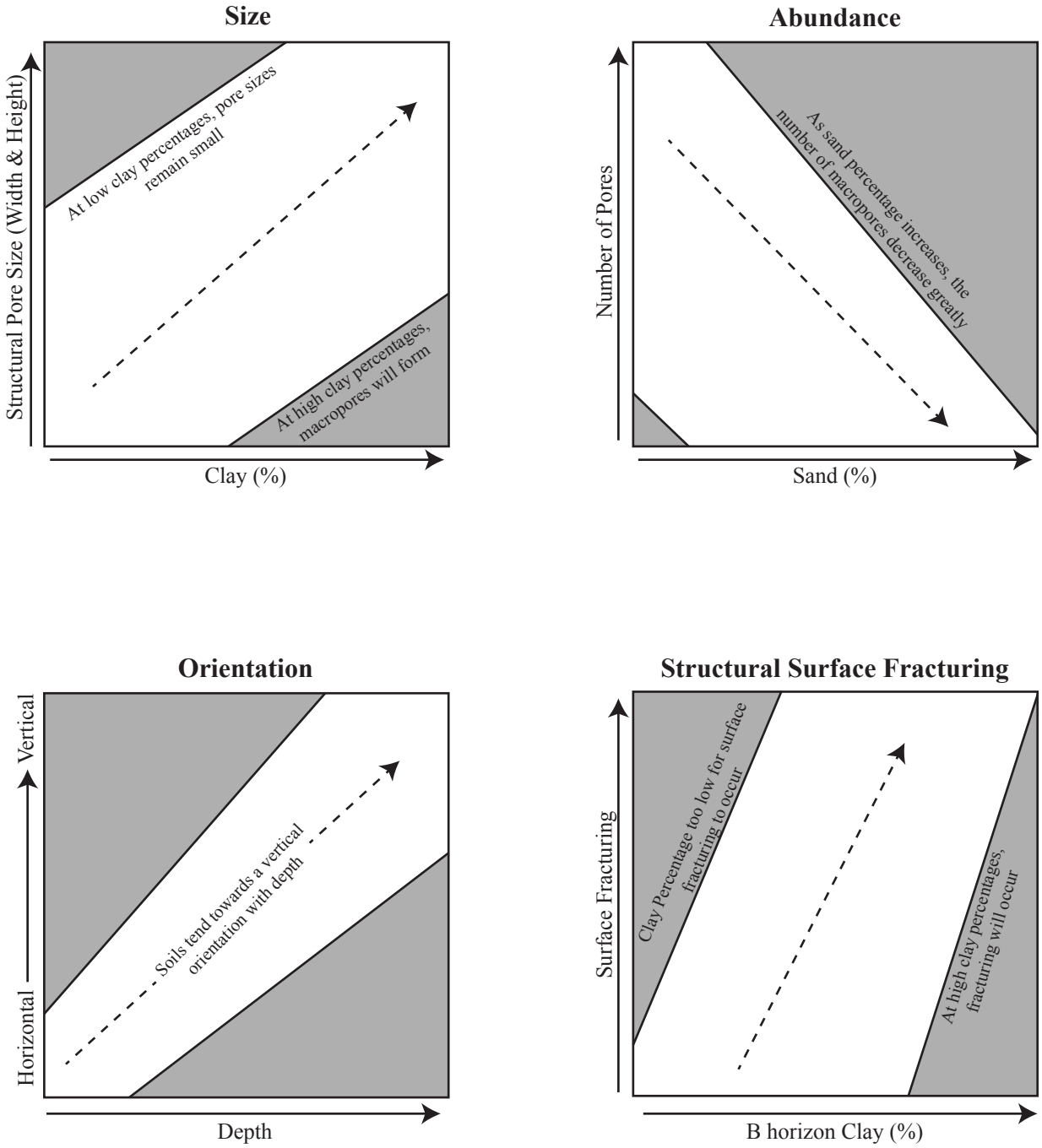

Fig. 7. Idealized constraints on soil structure. Each of the four metrics used in describing soil structure for this study are shown against the factor that most constrained that variable. Gray regions indicate areas where each measurement of soil structure becomes unlikely.

CHAPTER 3. DEVELOPMENT OF MACROPORE-BASED PEDOTRANSFER FUNCTIONS TO PREDICT SOIL HYDRAULIC PROPERTIES

ABSTRACT

The presence of macropores greatly influences soil hydraulic properties such as water retention and conductivity. In this study, I examined the potential of quantitative metrics of structural-induced macroporosity to predict soil hydraulic properties. Soils from northeastern Kansas were used in this study. The samples ranged in structure types, texture, and site management. Using a combination of multistripe laser triangulation (MLT) three-dimensional scanning technique to quantify macroporosity as well as basic soil physical properties, we were able to predict the field capacity, permanent wilting point, inflection point, and saturation water contents, saturated hydraulic conductivity, and effective porosity. The best prediction was observed for field capacity with silt content, coefficient of linear extensibility, and feret diameter as the most significant predictor variables. The use of MLT scanning opens up the possibility of better predicating hydraulic properties of the soil at the air-entry and capillary regions of the water retention curve.

INTRODUCTION

Soil hydraulic properties are influenced by macropores created through either abiotic (e.g., pores between prismatic structures) or biotic (e.g., root and earthworm channels) processes (Bouma and Wösten 1979; Ehlers, 1975). These macropores allow water and solutes to bypass the soil matrix and move deep into the soil profile (Jarvis, 2007; Kronvang et al., 1997). Experimental results indicate that pores with a cylindrical diameter at or larger than 300 μm can

have profound effects on preferential flow (e.g., Lin et al., 1997; Vervoort et al., 1999). Many of these macropores are created through the development of soil structure (Semmel et al., 1990).

Preferential flow paths serve as conduits which can move a considerable volume of liquid through the soil column without interacting extensively with the soil matrix. Thus, dissolved agricultural chemicals can bypass the soil matrix and rapidly move deep into the soil, simultaneously contaminating groundwater and being ineffective for their intended use (Jarvis et al., 2007). Bypass flow in soils due to macropores is common enough to arguably be the rule rather than the exception (Flury et al., 1994; Luo et al., 2010). Quantification of these macropores at the pedon scale, however, has remained elusive, requiring qualitative descriptions and semi-quantitative methods to be relied on for field descriptions of pores, root channels, and soil structure (e.g., Schoeneberger et al., 2012; Harden, 1982).

Saturated hydraulic conductivity (K_{sat}) is greatly affected by the presence of macropores. For example, abandoned earthworm channels, while comprising a very small percentage of the total soil pedon, can drain water at a rapid rate, up to 200 cm^3 per minute per channel (Ehlers, 1975; Steenhuis et al., 1990). When devoid of macropores, texture becomes the most important control of $K_{sat.}$ Coarser textured soils have higher K_{sat} values than finer-textured ones. However, many fine-textured soils have an expression of structure which create interpedal pores (i.e., those between structural peds) that increase K_{sat} to rates comparable to, or higher than, coarse textured soils (Vervoort et al., 1999).

Soil pore size-distributions can be quantified from the derivative of a function fit to data on water retention. Unimodal models (e.g., van Genuchten, 1980) are often used to characterize soil water retention; however, this type of function does not adequately capture the initial macropore drainage. For instance, at a potential of -10 cm, many soils exhibit a significant

amount of drainage, which is believed to be due to macropores (Wilson et al., 1992). Bimodal water retention functions can be used instead of unimodal ones because they better capture the nature of soil water retention in soils with macropores (Mallants et al., 1997). While bimodal water retention functions allow information about the abundance and size of macropores to be calculated, they do not give a description of the shape or orientation of those pores (Hunt et al. 2013). Additionally, determining water retention curves is time consuming and no single method can capture the entire range of retention points necessary to fit functions accurately (Or and Wraith, 2002). For example, hanging columns and tension tables can be used to determine potentials at water contents close to saturation, but can only measure one pressure potential at a time and have a practical measurement range limited to above field capacity. Pressure plates can be used to measure water content at potentials near field capacity and just above wilting point, but have a long equilibrium time for a single retention point. Dew point potentiameters can accurately measure retention points quickly (5-30 minutes per measurement) but only work at potentials well below the permanent wilting point (Gubiani et al., 2013). The combination of these methods can be used to generate data required to fit retention functions, but are both time and labor intensive, which often limits the number of soils that can feasibly be measured in an investigation.

A method for quantifying soil interpedal pores in the field was recently developed using a three-dimensional (3-D) laser scanner (Eck et al. 2013). In that study, multistripe laser triangulation (MLT) scanning was conducted on a soil with vertic properties (Oxyaquic Vertic Argiudoll) *in situ*, so interpedal pores could be captured digitally for analysis. Previous studies into MLT scanning have shown its ability to capture complex geometries of ichnofossils (Platt et

al. 2010) and the precise ability to measure volumes of soil clods in bulk density determination (Rossi et al., 2008).

Pedotransfer functions use basic soil data to predict more difficult to measure properties, including water retention (Wösten et al., 2001). Multiple studies have used descriptions of particle size to predict water retention (e.g., ROSETTA, Schaap et al., 2001; Rawls et al., 1982; Arya and Paris, 1981; Shein and Arkhangel'skaya, 2006). While particle size adequately predicts the nature soil water retention toward the adsorptive region of the curve, there is still a need to further understand bimodal soil water retention curves as they approach saturation. (Pachepsky and Rawls, 2003). I hypothesize that interpedal pores quantified by MLT can be used to predict parameters of the water retention curve in the air-entry and capillary regions (i.e., toward saturation) as well as K_{sat}, all of which are impacted by management decisions.

METHODS

Six sites in northeasten Kansas were used for this study. At each location, a soil pit was excavated and profiles were described following Schoeneberger et al. (2012). To prepare soils for scanning, profile faces were first straightened and cleaned using increasingly smaller hand tools to remove larger tool marks. Once profiles were straightened, their natural structure was revealed using a surficial flash freezing method (Hirmas, 2013). After preparation, soil profiles were left to air dry for 36 hours to allow for maximum expression of soil interpedal pores (Eck et al., 2013). MLT scanning was conducted at night due to interference issues from ambient light during scanning (Eck et al., 2013).

Subsequently, undisturbed soils were sampled by horizon for laboratory analysis. Cores (5 x 8 cm i.d.) were sampled from each horizon for laboratory determination of saturated

hydraulic conductivity and water retention. Additionally, bulk soil samples were taken for particle-size analysis and coefficient of linear extensibility (COLE) testing. In some cases, soil pits were closed before cores were sampled for determination of hydraulic properties. To obtain cores in those cases, large, 9 cm diameter cores were taken within 5 meters of the original soil pit using a hydraulic corer (Giddings Machine Company Inc, Windsor, CO). These cores were then cut and subsampled by horizon to obtain natural, undisturbed cores for analyses. Coefficient of linear extensibility values were measured in triplicate following the $COLE_{rod}$ method (Schafer and Singer 1976).

Saturated hydraulic conductivity was determined using a falling head benchtop device (KSat, Decagon Devices, Inc. Pullman, WA). To prepare each sample for K_{sat} determination, cores were saturated with a gypsum-saturated solution to prevent dispersion. Following manufacturers recommendations, rings were allowed to saturate a minimum of 24 hours. In well-structured, clay rich soils, water would begin to pool at the top of the core within one hour after being placed in water, indicating the presence of interpedal pores that were present in the field. Once samples were saturated, they were placed in the benchtop device, and a falling head method was used to measure K_{sat} for each sample. Triplicate measurements were taken for each sample, and triplicate core samples were used for each soil horizon.

Immediately after K_{sat} determination, cores were measured for water retention using an evaporative method (Schindler et al., 2010). This method uses two micro-tensiometers coupled with weight loss measurements over time to provide a high number of data points near the saturation end of the retention curve. To prepare samples, small boreholes were cut into one side of the soil core to provide a place for the micro tensiometers to fit into and provide contact with the soil. These tensiometers were attached to a base unit which connected to a computer that

could record readings of tension and weight of the sample over time until tensiometers reached cavitation. Cavitation typically occurred between four and eight days, depending on the texture of the samples. Sand-rich samples took the longest to reach cavitation due to the low unsaturated conductivity of such soils. Clay-rich soils took the shortest time.

Additional retention points were determined using pressure plates and by dewpoint potentiametry. For pressure plates, ground and air-dried soil samples were placed into rings on a ceramic plate, then saturated and placed into a chamber which was set at a given pressure; for samples in this study, -500 cm and -10,000 cm were used. After equilibrium was reached, samples were removed from the plate and gravimetric water content was determined on each sample.

For the chilled dew point method, samples were prepared as follows: using air-dried and ground samples, 5 grams of soil were measured and added to previously weighed stainless steel sample cups. After the soil was added, deionized water (DI) was added incrementally by pipette to the series of cups. Amounts added were: 0, 2, 4, 6, 8, 10, 14, 18, and 22 drops. After the DI was added, samples were thoroughly mixed to homogenize the soil and water mixture in each cup. Samples were covered and allowed to equilibrate for 16 hours. After initial equilibration, samples were stirred and covers were replaced for an additional 3 hours before running the analysis, per manufacturer recommendations. Pressure potentials were measured for each sample using a chilled dew point device (WP4C, Degacon Devices, Inc. Pullman, WA) and water content was determined gravimetrically after measurement.

Water retention functions can be either unimodal or multimodal (van Genucthen, 1980, Durner, 1994). A common unimodal function was proposed by van Genuchten:

$$S_e(h) = \frac{\theta - \theta_r}{\theta_s - \theta_r} = \left[\frac{1}{1 + (-\alpha h)^n}\right]^m \quad [1]$$

where h is the suction head (cm), S_e is the effective saturation, θ_s is the saturated water content, θ_r is the residual water content, θ is the water content at any given *h*, α is the inverse of the air-entry value, and *m* and *n* are fitting parameters. The common assumption that *m* = 1-1/*n* was utilized. This equation does an adequate job at describing water retention of soil, but does not capture the dual porosity domains commonly associated with well-structured soils. To address this issue, a bimodal version of the van Genuchten equation was developed by Durner (1994) and used in this work:

$$S_e(h) = w_1\left[\frac{1}{1 + (-\alpha_1 h)^{n_1}}\right]^{m_1} + w_2\left[\frac{1}{1 + (-\alpha_2 h)^{n_2}}\right]^{m_2} \quad [2]$$

The first domain is controlled by soil texture, while the second domain is closest to θ_s and dominated by soil structure. All parameters are the same as in the van Genuchten model, and *w* is used as a weighting factor for each domain.

For this project, a least square fitting method was adopted from previous work by utilizing Microsoft Excel's *solver* function (Anlauf 2014). This function was modified to fit a bimodal function rather than a unimodal one. Appendix A provides a complete description of this method.

Multiple points along the water retention curve are important in regards to soil management, including field capacity, permanent wilting point, and the water content at the inflection point of the structural water retention subcurve, also known as the S-index. All three of these points that can be derived using the water retention curve. The equation for the S-index is (Radcliffe and Šimůnek, 2010):

$$S(h) = \frac{{\alpha_2}^{n_2}\,(\theta_s - \theta_r) m_2 n_2 (-h)^{n_2 - 1}}{[1 + (-\alpha_2 h)^{n_2}]^{m_2 + 1}} \quad [3]$$

where the notation is the same as in Eq. [2]. In this work, the S-index is the slope of a water retention curve at the inflection point within the structural pore domain of a bimodal water retention curve. This index has been used as a measure of soil physical condition (Dexter, 2004) which is impacted by soil structure. Additionally, the water content at the S-index ($\theta_{s\text{-index}}$) has been identified as the optimum water content for tillage (Dexter and Bird 2001). Effective porosity was also calculated as the water content at saturation less the water content at field capacity, it is defined as the portion of the void space in a soil capable of transmitting a fluid (Gibb et al., 1984).

After soils were scanned using MLT, the resulting images were processed following Eck et al. (2013). Briefly, multiple sections from each horizon were scanned in the field. Images resulting from these scans were oriented and combined using software provided by the manufacturer (Scan Studio, NextEngine). Scans were then cropped to fit within the exact horizon boundaries and images were converted from 3-D to two dimensional (2-D) image types. After conversion, image analyses were conducted (ImageJ) and measurements of pores were extracted from each image. The results were then aggregated and used in this study. For a complete method, refer to Eck et al. (2013) or chapter 2 of this thesis.

RESULTS

Laboratory Results

Results for particle-size distribution are shown in Fig. 1. The majority of the samples had textures between silty clay and silty clay loam, which is representative of soils in northeastern Kansas (Soil Survey Staff, 2015). Coarse and fine textured soils were also sampled in this work

to provide a wider range of textures (Table 1). The range of soil textures also corresponded with a range of structures (Table 1). Saturated hydraulic conductivity values were also highly variable, ranging over three orders of magnitude (< 1 cm d^{-1} to over 2000 cm d^{-1}) (Table 1). Coefficient of linear extensibility values ranged greatly between the samples, from 0.012 to 0.099 (Table 1), with 0-0.03 representing a slight shrink-swell hazard and > 0.09 representing a very severe shrink-swell hazard (Schafer and Singer, 1976). Coefficient of linear extensibility is a measurement of shrink-swell potential, which can affect the type of soil structure, fracturing of soil, and density and expression of pores present within each soil type (Chapter 2 of this thesis).

MLT Results

A myriad of structural metrics were derived from 3-D scans used in this study. For a complete listing of metrics, see Eck et al. (2013). Variables that significantly correlated with hydraulic properties of interest were used for multivariate linear regression. Size factors which were utilized in this study included feret diameter, average height and width of pores, and major and minor ellipse axes. Form factor, a shape metric was also considered as well as relative surface area of the pores. An example of a resulting digital image from MLT scans is shown in Fig. 2.

Feret diameter is defined as the maximum caliper size of a given soil pore. Resulting average feret diameters are given in Table 1. The largest feret diameters were from the Hill Field profile (Table 1). Very high COLE values at this profile meant that the pores opened up to a maximum extent as they dried. The lowest values came from the Robinson Tract (Table 1). Here, sandy soil dominated the majority of the profile, but at the Bt1 horizon, the feret diameter value increased, indicating an increase of soil structure.

Height and width of pores measure the pore sizes on a strict x and y axis; width measures along the x-axis and height measures along the y-axis. Average height and width values are given in Table 1. For the majority of profiles the average height and width were similar values, indicating that pores were equally distributed long and tall. In the 2Btk horizon of the Hill Field profile, the difference between height and width was only 0.2 mm. These values being nearly identical indicates that the pores were equally distributed tall and wide, which would be typical of a subangular or angular blocky soil ped type. This is supported from field descriptions as the peds of the 2Btk horizon were medium sized subangular blocky. In the Bt2 horizon of the Native Medicinal Plant Research Garden, the height was an average of 1.4 mm longer than the width. Very coarse and coarse sized prismatic structure was noted in the description, which would result in a larger height value.

Major and minor ellipse axis were also calculated; results are given in Table 1. Major ellipse axis is the length of the major axis of an ellipse fit around each pore of a profile scan; minor ellipse is the length of the minor axis. These measurements give the idealized longest and shortest length of a pore and give a generalized average size of pores. Relative surface area, or relative fracture surface, is a measurement of the space the macropores occupy compared to the entire soil horizon. The higher the value, the more macropores exist. Form factor is a derived metric that takes into account pore area and perimeter. This is a basic shape descriptor that has been used in other image processing studies (Aligizaki, 2006). Form factor gives a general idea of how much area pores have and over what space they occupy. Results are all shown in Table 1. In general, the highest relative surface area values were found in the A horizons of each profile. The only exception was the Konza Agriculture field. In that profile, the Bt1 horizon had the highest value. This could indicate that organic matter is a controlling factor to the total

amount of pores which will be present in a soil. However, when soils are under tillage, the displacement removes the porosity that would be found in a natural soil.

Water Retention

Resulting water retention curve parameters are shown in Table 2. Retention curves were plotted per site and shown, by profile, in Fig. 3. Coefficients of determination (R^2) were calculated using the square value of the excel correlation function (CORREL) between measured and calculated values of water content at each measured pressure head to assess how well the fitting method reflected measured data points. The coefficient of determination values are given in Table 2. Excluding the Bt1 horizon of the Konza Agriculture field, all R^2 values were above 0.9, indicating satisfactory fits with the measured data points. At the Bt1 horizon, insufficient data points precluded the model from a better fit.

Water contents of interest were extracted from each curve. Major points included field capacity, permanent wilting point and the water content at the S-index. Field capacity and permanent wilting point, were defined as -330 cm and -15,000 cm, respectfully, the water content at those points are shown in Table 3. The water content at the inflection point was calculated and is shown in Table 3, along with water contents at field capacity and permanent wilting point. Effective porosity was also calculated and included in Table 3.

Field capacity water content values ranged from 0.176 in the Robinson Ap horizon to 0.487 in the Bt2 horizon of the Konza Core site (Table 3). At the Robinson tract, sand was the dominant texture, which has a low matric potential and results in a rapid decrease in water content at low pressure potentials. Conversely, the Bt2 horizon of the Konza core has a high COLE value (0.101, Table 1) indicating a large amount of smectitic clays which will hold on to a

higher amount of water at increasingly negative pressure potentials. Similar field capacity water contents to the Konza Core are in the Bluff Field, Hill Field, and Konza Agriculture Field. All of these profiles have similar textures (silty clay) and structures (subangular blocky) to the Konza Core (Table 1).

Permanent wilting point water content values ranged from 0.021 in the Robinson A horizon up to 0.395 in the Konza Core Bt2 horizon (Table 3). The sand dominated profile of the Robinson tract does not permit water to be held to grains strongly when pressure potentials become increasingly negative, which becomes problematic for management when water is not readily available for irrigation or from rainfall. At the permanent wilting point of the Konza Core, as well as the Konza Agriculture field, values are in the 0.3 range, indicating that, while water is present, it is not available to plants due to the high matric potential of the clays in those profiles. Water content at the S-index ranged from 0.263 in the Native Medicinal Plant Research Garden Ap horizon to 0.646 in the Konza Core A horizon (Table 3).

Water content at saturation ranged from 0.380 in the Robinson Tract Bt1 horizon to 0.696 in the Konza Core A horizon (Table 3). Higher saturation values would indicate a higher amount of total porosity available. Generally, organically rich horizons have the highest total porosity, as is the case with the Konza Core profile. Additionally, in natural environments, such as the Konza Core and Hill Field, porosity is even higher in upper horizons compared to a disturbed site like the Konza Agriculture Field. When soils are tilled, much of the natural porosity is destroyed and soils will become more densely packed over time. Effective porosity ranged from 0.074 in the Btky horizon of the Konza Core site to 0.386 in the E2 horizon of the Robinson Tract (Table 3). At a higher effective porosity, more pore space is present, which can be indicative of well-graded soil structure.

Creating Pedotransfer Functions

For each hydraulic property measured (K_{sat}, θ_s, θ_{fc}, θ_{pwp}, $\theta_{s\text{-}index}$, effective porosity), a multiple linear regression was run using a combination of physical properties of the soil and metrics measured for each horizon using MLT 3-D scanning. Spearman and Pearson correlation coefficients were calculated and only variables which significantly correlated with hydraulic properties were chosen for regression analyses. Backwards step-wise multiple linear regressions were conducted using SPSS (IBM SPSS 21). Variables were significant at the $\alpha = 0.05$ level. Variance inflation factor was used to ensure multicollinearity was not present in the multiple linear regressions.

Resulting regressions, their coefficient of determinations, and mean standard error for each regression is shown in Table 4. Beta weights for each regression are also included in Table 4. Model output compared to measured values for each regression used is shown in Fig. 4. The coefficients of determination were all above 0.5. The highest coefficient (0.812) was for field capacity. Mean standard error was calculated as the sum of the difference of the actual value and predicted value divided by the number of samples. All of these values were below 0.03, indicating a small error and low variance between measured and predicted values of each regression.

DISCUSSION

The goal of this study was to predict important soil hydraulic properties from typically measured physical properties and quantified soil structure. These results show that relationships can be established between metrics derived from MLT scanning, basic properties, and hydraulic

properties. As the multivariate regression analysis showed, six different hydraulic properties that are each time consuming in their own right were successfully predicted in this work.

Saturated Hydraulic Conductivity

The three factors which predicted K_{sat} were bulk density, percent silt, and form factor. Silt had the highest beta weight of the predictor variables. The silt percentage of these soils ranged from less than 5% to over 70%. Particle-size distribution affects water flux, as coarser soils will move water rapidly compared to unstructured fine soils.

Bulk density was the next highest beta weight. The packing of particles has a large role in how quickly water will move through the soil, and how transmissible it is when all the pores are filled with water. Sample with low bulk density (e.g., Konza Core A horizon, 0.806 g cm^{-3}) have an increased pore space resulting in high K_{sat} values (1280 cm d^{-1}). Conversely, samples with higher bulk densities indicate that the arrangement of particles are more compact and there is less pore space to move water (e.g., Konza Core Btkss horizon, 1.42 g cm^{-3}). This also could mean that a soil either has less structure and water has a more tortuous path, resulting in a low K_{sat} (10.8 cm d^{-1}), or pores close when saturated.

The last variable that was a significant predictor of K_{sat} was form factor. Form factor is a shape descriptor derived from MLT scanning. The relationship with K_{sat} indicates that soil structure does affect soil water flux. Soil structure can form conduits for water to move through a profile at a faster rate than in a similar soil without structure present (Jarvis, 2007).

Water Content at Saturation

At saturation, the entire pore space of a soil sample is filled with water rather than a mixture of air and water. Three MLT derived shape parameters and bulk density were used to

predict θ_s. Minor ellipse axis had the highest beta weight, followed by width, major ellipse axis, and bulk density. The major and minor ellipse give a general average of pore sizes, which will affect the total porosity of a soil, so it is not surprising that they also helped to predict the total pore space available in a sample for water to occupy. The width factor is a generalization of how large (wide) pores are and how much water can be stored in a given soil when saturated. Finally bulk density was a predictive factor in estimating θ_s, as how densely solids are packed into an area dictates the percent of the soil which can be occupied by water or air.

Field Capacity

Three factors were used in the regression for field capacity: silt, COLE and feret diameter. Coefficient of linear extensibility had the highest beta weight, followed by silt and finally feret diameter. Soils with a high COLE value indicates that they contain a large percentage of expansive clays. When hydrated, these soils expand and can hold much more water than non-expansive ones (Aina and Periaswamy, 1985). Silt was the next highest beta weight for predicting field capacity. Particle-size distribution will affect how water will move past, or interact with soils. In soils with low matric potentials (i.e., sand) water will flow freely past the particles, but in soils with high matric potentials (i.e., clay) water will cling to the particles and move slowly. The final predictor was feret diameter. This size metric indicates that soil structure has a role in soils reaching field capacity. The structural pores are the ones which allow water to move most freely by the effect of gravity, and having feret diameter predict field capacity indicates that this measurement is capturing such pores.

Permanent Wilting Point

Permanent wilting point, the water content at the lowest water potential of soils which can provide available water to plants (Hillel 1980), was predicted using width, feret diameter, minor ellipse, height, and COLE. In this multivariate regression, many of the beta weights were two or three deviations apart, indicating their influence on the prediction was quite large, this is not uncommon with multilinear regression when there is a large spread of data. In this case, permanent wilting point ranged in water content from almost 0 up to 0.35, a comparatively large range considering pore space rarely is greater than 0.5 (Hillel, 1980). The size of pores seemed to be the largest factor in predicting permanent wilting point because of the four factors, three of them were MLT size metrics. This is interesting because the size of pores were hypothesized to be more influential closer to saturation. Additionally, particle-size distribution was hypothesized to be more influential in predicting permanent wilting point. The final variable used in the regression was COLE. Coefficient of linear extensibility inherently describes soil texture, as higher values of COLE contain a higher amount of fine clay and ones with low values primarily contain sand.

Water Content at S-Index

The water content at the inflection point of the structural domain was best explained using height, relative surface area, and feret diameter. The three variables all describe the size or relative surface fracture of the soil. This finding is important because only structural metrics were used to find this point, which has been hypothesized to reflect soil structure (Dexter, 2004). At the inflection point, soil structure no longer contributes significantly to water movement. The fact that this was predicted only using quantified structure metrics indicates that the MLT

technique is capturing structural pores and provides a step forward in the development of pedotransfer functions.

Effective Porosity

The effective porosity, or range of the soil which can transmit fluid (Gibb et al., 1984) interestingly did not depend on any measured structural characteristics. Instead, it relied primarily on silt, midpoint depth and COLE. While none of the factors were direct measurements of soil structure, each is related to it. The percent of silt varied in the samples from near zero to very high (70%); and with increased and decreased silt values, ped types also changed significantly. Granular horizons dominate at the top of profiles and subangular blocky and prismatic structures dominate in lower horizons. Finally, COLE reflects the shrink-swell potential in soils. Active (e.g., mobile smectitic) clays are present in horizons with high COLE values. With higher clay activity, more soil structure will form due to the development of pressure faces. (Schaetzl and Anderson, 2005, Utomo and Dexter, 1981). This fracturing of the soil will make structural conduits for liquids to move through.

CONCLUSION

In this work, pedotransfer functions were established for soil hydraulic properties using soil physical measurements and MLT-quantified soil structure. Field capacity was best predicted in this work, which was an intriguing find as it is difficult to model. These functions should be verified on a broader scale, but, nonetheless, show enormous promise in predicting hydraulic properties. The capability of predicting such properties is expected to improve understanding of how hydraulic properties are related to soil structure.

REFERENCES

Aina, P.O., S.P. Periaswamy. 1985. Estimating available water-holding capacity of western Nigerian soils from soil texture and bulk density, using core and sieved samples. Soil Science. 140:55-58.

Aligizaki, K.K. 2006. Pore structure of cement-based materials: testing, interpretation and requirements. Taylor & Francis. 1-23.

Anlauf, R. 2014. Using the EXCEL solver function to estimate the van Genuchten parameters from measured pF/wate content values. Excel spreadsheet retrieved from www.al.hs-osnabrueck.de/anlauf.html on [7-18-2015].

Arya, L.M., and J.F. Paris. 1981. A physicoempirical model to predict the soil moisture characteristic from particle-size distribution and bulk density data. Soil Science Society of America Journal. 45:1023-1030.

Bouma, J., and J.H.L. Wösten. 1979. Flow patterns during extended saturated flow in two undisturbed swelling clay soils with different macrostructures. Soil Science Society of America Journal. 43:16-22.

Dexter, A.R. 2004. Soil physical quality Part I. theory, effects of soil texture, density, and organic matter, and effects on root growth. Geoderma 120:201-214.

Dexter, A.R, N.R.A. Bird. 2001. Methods for predicting the optimum and the range of soil water contents for tillage based on the water retention curve. Soil & Tillage Research 57:203-212.

Durner, W. 1994. Hydraulic conductivity estimation for soils with heterogeneous pore structure. Water Resource Research. 30:211-223.

Eck, D.V., D.R. Hirmas, and D. Giménez. 2013. Quantifying soil structure from field excavation walls using multistripe laser triangulation scanning. Soil Science Society of America Journal. 77:1319-1328.

Ehlers, W. 1975. Observations on earthworm channels and infiltration on tilled and untilled loess soil. Soil Science.119:242-249.

Flury, M., H. Fluhler, W.A. Jury and J. Leuenberger. 1994. Susceptability of soils to preferential flow of water: a field study. Water Resource Research. 30:1945-1954.

Gibb, J.P., M.J. Barcelona, J.D. Ritchey, and M.H. LeFaivre. 1984. Effective porosity of geologic materials first annual report. Illinois Department of Energy and Natural Resources State Water Survey Division SWS Contract Report 351: 1-40.

Gubiani, P.I., J.M. Reichert, C. Campbell, D.J. Reinert, and N.S. Gelain. 2013. Assessing errors and accuracy in dew-point potentiometer and pressure plate extractor measurements. Soil Science Society of America Journal. 77:19-24.

Harden, J.W. 1982. A quantitative index of soil development from field descriptions: Examples from a chronosequence in central California. Geoderma. 28:1-28.

Hillel, D. 1980. Fundamentals of soil physics. Academic Press. 265-284.

Hirmas, D.R. 2013. A simple method for removing artifacts from moist fine-textured soils faces. Soil Science Society of America Journal. 77:591-593.

Hunt, A.G., R.P. Ewing, and R. Horton. 2013. What's wrong with soil physics? Soil Science Society of America Journal. 77:1877-1887.

Jarvis, N.J. 2007. A review of non-equilibrium water flow and solute transport in soil macropores: principles, controlling factors and consequences for water quality. European Journal of Soil Science. 58:523-546.

Jarvis, N., M. Larsbo, S. Roulier, A. Lindahl, and L. Persson. 2007. The role of soil properties in regulating non-equilibrium macropore flow and solute transport in agricultural topsoils. European Journal of Soil Science. 58:282-292.

Kim, J.G., C. Chon, and J. Lee. 2004. Effect of structure and texture on infiltration flow pattern during flood irrigation. Environmental Geology. 46:962-969.

Kronvang, B., A. Laubel, and R. Grant. 1997. Suspended sediment and particulate phosphorus transport and delivery pathways in an arable catchment, Gelbæk stream, Denmark. Hydrological Processes. 11:627-642.

Lin, H.S., K.J. McInnes, L.P. Wilding, and C.T. Hallmark. 1997. Low tension water flow in structured soils. Canadian Journal of Soil Science. 77:649-654.

Luo, L., H. Lin, J. Schmidt. 2010 Quantitative relationships between soil macropore characteristics and preferential flow and transport. Soil Science Society of America Journal. 74:1929-1937.

Mallants, D., P. Tseng, N. Toride, A. Timmerman, and J. Feyen. 1997. Evaluation of multimodal hydraulic functions in characterizing a heterogeneous field soil. Journal of Hydrology. 195:172-199.

Or, D., and J.M. Wraith. 2002. Soil water content and water potential relationships. Soil physics companion. 49-84.

Pachepsky, Y.A., and W.J. Rawls. 2003. Soil structure and pedotransfer functions. European Journal of Soil Science. 54:443-451.

Platt, B.F., S.T. Hasiotis, and D.R. Hirmas. 2010. Use of low-cost multistripe laser triangulation (MLT) scanning technology for three-dimensional, quantitative paleoichnological and neoichnological studies. Journal of Sedimentary Research. 80:590-610.

Radcliffe, D.E., and J. Šimůnek. 2010. Soil physics with HYDRUS: modeling and applications. Boca Raton, FL. CRC press. p.68-69

Rawls, W.J., D.L. Brakensick, and K.E. Saxton. 1982. Estimation of soil water properties. Transactions of the ASAE. 25:1316-1320&1328.

Rossi, A.M., D.R. Hirmas, R.C.Graham, and P.D. Sternberg. 2008. Bulk density determination by automated three-dimensional laser scanning. Soil Science Society of America Journal. 72:1591-1593.

Schaap, M.G., F.J. Leij, and M. Th. van Genuchten. 2001. ROSETTA: a computer program for estimating soil hydraulic parameters with hierarchical pedotransfer functions. Journal of Hydrology. 251:163-176.

Schaetzl, R.J., and S. Anderson. 2005. Soils: genesis and geomorphology. Cambridge University Press. 83-92.

Schafer, W.M., and M.J. Singer. 1976. A new method of measuring shrink-swell potential using soil pastes. Soil Science Society of America Journal. 40: 805-806.

Schindler, U., W. Durner, G., and von Unold, L. Müller. 2010. Evaporation method for measuring unsaturated hydraulic properties of soils: extending the measurement range. Soil Science Society of America Journal. 74:1071-1083.

Schoeneberger, P.J., D.A. Wysocki, E.C. Benham, and Soil Survey Staff. 2012. Field Book for Describing and Sampling Soils, Version 3.0. Natural Resources Conservation Service, National Soil Survey Center, Lincoln, NE.

Semmel, H., R. Horn, U. Hell, A.R. Dexter, and E.D. Schulze. 1990. The dynamics of soil aggregate formation and the effect on soil physical properties. Soil Technology 3:113-129.

Shein, E.V. and T.A. Arkhangel'skaya. 2006. Pedotransfer functions: state of the art, problems, and outlooks. Eurasian Soil Science. 39:1205-1217.

Soil Survey Staff, Natural Resources Conservation Service, United States Department of Agriculture. U.S. General Soils Map (STATSGO2). http://sdmdataaccess.nrcs.usda.gov/. Accessed [9/6/2015].

Steenhuis, T.S., W. Staubitz, M.S. Andreini, J. Surface, T.L. Richard, R. Paulsen, N.B. Pickering, J.R. Hagerman, and L.D. Geohring. 1990. Preferential movement of pesticides and tracers in agricultural soils. Journal Irrigation and Drainage Engineering. 116:50-66.

Utumo, W.H. and A.R. Dexter. 1981. Soil friability. Journal of Soil Science. 32:203-213.

van Genuchten, M.Th. 1980. A closed-form equation for predicting the hydraulic conductivity of unsaturated soils. Soil Science Society of America Journal. 44:892-898.

Vervoort, R.W., D.E. Radcliffe, and L.T. West. 1999. Soil structure development and preferential solute flow. Water Resource Research. 35:913-928.

Wilson, G.V., P.M. Jardine, and J.P Gwo. 1992. Modeling the hydraulic properties of a multi-region soil. Soil Science Society of America Journal. 56:1731-1737.

Wösten, J.H.M., Ya.A. Pachepsky, and W.J. Rawls. 2001. Pedotransfer functions: bridging the gap between available basic soil data and missing soil hydraulic characteristics. Journal of Hydrology. 251:123-150.

Table 1. Selected properties and measured MLT metrics of each soil sample used in this study.

Horizon	Depth	Texture†	Structure‡	K_{sat}§	Bulk Density	COLE¶	Feret Diameter	Height	Width	Major Ellipse	Minor Ellipse	Relative Surface Area	Form Factor
	cm			cm d^{-1}	g cm^{-3}		mm					mm^{-1}	
						Konza Agriculture Field							
Ap	0-12	sicl	1co cdy	418 ± 30	1.06±0.03	0.044±0.00	7.005	5.148	4.828	5.840	2.2603	0.081	0.459
Bt1	12-31	sicl	2f sbk	156 ± 735	1.29±0.03	0.098±0.04	7.145	5.289	4.893	5.871	2.2614	0.207	0.495
Bt2	31-54	sic	1m pr/2m sbk	53.8 ± 20	1.37±0.06	0.091±0.02	7.059	5.146	5.134	5.835	2.3744	0.105	0.477
Bt3	54-89	sic	1m pr/2m sbk	23.6 ± 8.4	1.49±0.00	0.106±0.02	7.587	5.563	5.304	6.080	2.3976	0.108	0.501
Btss	89-119	sic	1co pr/2m sbk	82.3 ± 27	1.41±0.06	0.108±0.03	7.247	5.259	5.258	5.889	2.4742	0.115	0.510
						Konza Core							
A	0-10	sil	2f gr	1280 ± 874	0.81±0.08	0.042±0.01	8.634	6.211	7.007	6.685	3.4454	0.281	0.465
Bt1	10-26	sicl	1m pr/2m sbk	465 ± 271	1.08±0.09	0.112±0.00	6.773	5.278	4.737	5.512	2.5262	0.125	0.503
Bt2	26-66	sicl	1co pr/2m sbk	3.08 ± 2.0	1.29±0.01	0.110±0.02	6.731	5.167	4.675	5.571	2.3815	0.065	0.531
Btkss	66-89	sicl	1co pr/2m sbk	10.8 ± 20	1.42±0.02	0.071±0.02	6.027	4.297	4.308	5.029	2.1000	0.028	0.548
Btky	89-132	sicl	1co pr/2m sbk	345 ± 717	1.43±0.05	0.068±0.01	5.760	4.689	3.527	5.099	2.0340	0.018	0.564
						Hill Field							
A1	0-13	sicl	2m gr	2260 ± 176	1.08±0.08	0.091±0.02	9.693	7.507	7.317	7.257	3.6817	0.299	0.440
A2	13-28	sicl	2vf sbk	573 ± 463	1.34±0.17	0.09±0.01	7.413	6.003	5.101	5.917	2.7214	0.197	0.472
Bt1	28-43	sicl	2f sbk	1210 ± 788	1.30±0.08	0.103±0.00	7.007	5.543	4.666	5.674	2.3930	0.160	0.486
Bt2	43-76	sicl	2m sbk	882 ± 3158	1.14±0.14	0.101±0.00	7.620	5.948	5.322	6.052	2.6934	0.179	0.492
2Bt3	76-101	c	1m sbk	146 ± 181	1.03±0.04	0.083±0.02	7.626	5.832	5.423	6.017	2.6845	0.168	0.499
2Btk	101-121	c	1m sbk	168 ± 2318	1.23±0.11	0.073±0.02	7.734	5.826	5.602	6.134	2.7143	0.174	0.507
						Native Medicinal Plant Research Garden							
Ap	0-8	sil	3cogr, 2f,m sbk	1050 ± 55	1.03±0.01	0.017±0.01	5.712	2.500	4.232	4.851	1.3982	0.024	0.445
A	8-20	sil	1m,co pr	91.7 ± 211	1.09±0.07	0.036±0.01	4.300	2.853	2.822	3.749	1.5040	0.003	0.549
AB	20-33	sil	2mpr	227 ± 4.0	1.12±0.04	0.042±0.02	3.686	3.215	2.320	3.156	1.6712	0.003	0.365
Bt1	33-67	sicl	3copr	146 ± 46	1.08±0.07	0.040±0.01	4.899	3.668	2.593	4.375	1.5256	0.015	0.541
Bt2	67-101	sil	3co,vc pr	862 ± 385	1.13±0.03	0.021±0.00	4.491	3.770	2.303	4.060	1.5912	0.009	0.413
						Robinson Tract							
Ap	0-8	sl	2f,m sbk/ 2m, co gr	1730 ± 104	1.06±0.12	0.012±0.00	4.984	3.416	3.826	4.207	1.8883	0.146	0.445
A	8-30	ls	1m,co sbk	1480 ± 34	1.31±0.03	0.012±0.00	3.880	2.834	2.622	3.441	1.5115	0.018	0.549
E1	30-42	ls	1msbk	2030 ± 136	1.32±0.03	0.012±0.00	4.934	3.989	2.018	4.342	1.2207	0.004	0.365
E2	42-69	ls	1msbk	747 ± 89	1.45±0.05	0.012±0.00	4.417	3.496	2.258	3.877	1.5213	0.003	0.541
Bt1	69-107	scl	2vc,co,m,f pr/ 2f,m abk	456 ± 95	1.65±0.15	0.023±0.01	5.171	4.214	2.641	4.539	1.4245	0.022	0.413
						Bluff Field							
A	0-5	sil	2m,co gr, 1,2 m sbk, 1 mpl	1310 ± 183	0.97±0.03	0.052±0.01	5.533	3.760	3.945	4.618	1.9441	0.230	0.435
AB	5-20	sicl	2m pr/ 2m-co sbk	7.23 ± 1.5	1.24±0.24	0.080±0.02	5.517	3.962	3.388	4.672	1.8037	0.098	0.469
Bt1	20-30	sic	2m pr/ 2f-m abk	12.1 ± 4.7	1.13±0.04	0.12±0.02	4.913	3.376	3.325	4.204	1.6674	0.121	0.464
Bt2	30-56	sic	3m-vc pr/3f-co abk	0.84 ± 1.4	1.24±0.14	0.106±0.01	5.348	3.880	3.320	4.619	1.8585	0.107	0.500
Bt3	56-76	sic	1mpr/3m-co abk	40.3 ± 0.6	1.51±0.11	0.099±0.01	4.784	3.533	3.036	4.168	1.7738	0.039	0.559
Bt4	76-102	sic	3co-vc abk/2mabk	43.3 ± 6.7	1.46±0.23	0.105±0.02	4.721	3.340	3.013	4.160	1.5660	0.050	0.490

† Text, Texture; sil, silt loam; sic, silty clay; sicl, silty clay loam; ls, loamy sand; scl, sandy clay loam; cl, clay loam; c, clay.

‡ 1, weak; 2, moderate; 3, strong; vf, very fine; f, fine; m, medium; co, coarse; vc, very coarse; gr, granular; sbk, subangular blocky; abk, angular blocky; pr, prismatic; weg, wedge; cdy, cloddy; /, parting to.

§ K_{sat}, Saturated Hydraulic Conductiviy

¶ COLE, Coefficient of Linear Extensibility

Table 2. Water retention curve parameters derived from fits to the water retention data.

Horizon	Depth	α_1	α_2	n_1	n_2	m_1	m_2	w_1	w_2	θ_r	R^2 Fit
	cm	——— cm^{-1} ———								$cm^3\ cm^{-3}$	
					Konza Agriculture Field						
Ap	0-12	0.0208	0.0203	1.0002	1.6480	0.0002	0.3932	0.2679	0.6936	0.050	0.9487
Bt1	12-31	0.0138	1.8117	1.4597	1.0678	0.3149	0.0635	0.1407	0.9141	0.001	0.7549
Bt2	31-54	0.0502	3.6846	1.0782	1.1409	0.0726	0.1235	1.0227	0.0001	0.022	0.9802
Bt3	54-89	0.0029	0.2047	1.5596	1.0437	0.3588	0.0418	0.4753	0.5223	0.050	0.9982
Btss	89-119	0.1894	0.0030	1.0776	1.2987	0.0720	0.2300	0.5110	0.4808	0.050	0.9968
					Konza Core						
A	0-10	0.0012	0.1231	1.6194	1.5121	0.3825	0.3387	0.5261	0.4956	0.050	0.9968
Bt1	10-26	0.3325	0.0010	1.1209	1.0001	0.1079	0.0001	1.0343	0.0003	0.001	0.9943
Bt2	26-66	0.0037	2.4436	2.0000	1.0068	0.5000	0.0067	0.2455	0.7621	0.001	0.9943
Btkss	66-89	0.0076	0.0107	1.0132	1.6427	0.0130	0.3912	0.5875	0.3963	0.001	0.9878
Btky	89-132	0.0735	0.0012	1.3847	2.0000	0.2778	0.5000	0.1373	0.8613	0.001	0.9975
					Hill Field						
A1	0-13	0.0010	0.0860	1.6120	1.8907	0.3796	0.4711	0.6364	0.3660	0.001	0.9969
A2	13-28	1.0000	0.1221	1.0000	1.1547	0.0000	0.1340	0.0010	1.0000	0.001	0.9947
Bt1	28-43	0.0998	0.0156	2.0000	1.1067	0.5000	0.0964	0.2268	0.7911	0.001	0.9962
Bt2	43-76	0.1885	1.4340	1.1655	1.0439	0.1420	0.0420	0.4835	0.5460	0.015	0.9985
2Bt3	76-101	0.0030	0.0606	1.2264	1.2608	0.1846	0.2069	0.6734	0.3249	0.001	0.9969
2Btk	101-121	0.0639	1.5000	1.2079	1.0001	0.1721	0.0001	0.6699	0.3238	0.001	0.9950
					Native Medicinal Plant Research Garden						
Ap	0-8	0.0290	0.0015	1.2350	2.0000	0.1903	0.5000	0.6500	0.3380	0.001	0.9983
A	8-20	0.4467	0.0054	2.0000	1.4716	0.5000	0.3205	0.0270	0.9739	0.015	0.9964
AB	20-33	0.0093	1.5000	1.3230	1.3973	0.2441	0.2843	0.9343	0.0836	0.015	0.9990
Bt1	33-67	0.0028	0.0317	2.0000	1.1366	0.5000	0.1202	0.6257	0.3751	0.008	0.9882
Bt2	67-101	0.3159	0.0253	1.1960	1.3034	0.1639	0.2328	0.2776	0.6866	0.015	0.9899
					Robinson Tract						
Ap	0-8	0.0012	0.0484	1.1173	1.4751	0.1050	0.3221	0.0760	0.9891	0.001	0.9696
A	8-30	0.0010	0.0454	1.5030	2.0000	0.3347	0.5000	0.1547	0.9473	0.001	0.9664
E1	30-42	0.0706	1.5000	1.5098	1.0001	0.3376	0.0001	1.1250	0.0001	0.015	0.9619
E2	42-69	0.0707	0.0677	1.5200	1.4610	0.3421	0.3155	0.3509	0.7356	0.001	0.9592
Bt1	69-107	0.5536	0.0049	1.1961	1.2378	0.1640	0.1921	0.2365	0.7834	0.001	0.9861
					Bluff Field						
A	0-5	0.0022	0.2505	1.3136	1.2850	0.2387	0.2218	0.6821	0.3252	0.001	0.9983
AB	5-20	0.0010	0.0252	1.2757	1.2433	0.2161	0.1957	0.5865	0.4088	0.001	0.9962
Bt1	20-30	0.0331	0.0044	1.1860	1.1644	0.1568	0.1412	0.2665	0.7319	0.001	0.9959
Bt2	30-56	0.0079	0.0064	1.2072	1.8977	0.1716	0.4730	0.8251	0.1483	0.001	0.9957
Bt3	56-76	0.0070	1.5000	1.2092	1.0001	0.1730	0.0001	0.9900	0.0001	0.015	0.9946
Bt4	76-102	0.0034	1.4989	1.2457	1.1330	0.1972	0.1174	0.8136	0.2328	0.001	0.9896

Table 3. Water contents at field capacity (fc), permenant wilting point (pwp), and s-index point for the sites studied.

Horizon	Depth	θ_{fc}	θ_{pwp}	$\theta_{s\text{-}index}$	θs	Effective Porosity†
	cm			$g\ g^{-1}$		
			Konza Agriculture Field			
Ap	0-12	0.307	0.209	0.578	0.600	0.294
Bt1	12-31	0.360	0.278	0.470	0.520	0.160
Bt2	31-54	0.398	0.311	0.459	0.481	0.083
Bt3	54-89	0.382	0.233	0.410	0.460	0.078
Btss	89-119	0.363	0.233	0.394	0.450	0.087
			Konza Core			
A	0-10	0.413	0.131	0.646	0.696	0.283
Bt1	10-26	0.347	0.230	0.529	0.592	0.245
Bt2	26-66	0.487	0.395	0.540	0.550	0.063
Btkss	66-89	0.418	0.322	0.523	0.560	0.142
Btky	89-132	0.386	0.038	0.338	0.460	0.074
			Hill Field			
A1	0-13	0.408	0.102	0.621	0.660	0.252
A2	13-28	0.339	0.200	0.590	0.600	0.261
Bt1	28-43	0.384	0.268	0.559	0.580	0.196
Bt2	43-76	0.362	0.276	0.530	0.540	0.178
2Bt3	76-101	0.419	0.210	0.555	0.565	0.146
2Btk	101-121	0.366	0.269	0.530	0.540	0.174
			Native Medicinal Plant Research Garden			
Ap	0-8	0.286	0.081	0.263	0.420	0.134
A	8-20	0.270	0.072	0.358	0.400	0.130
AB	20-33	0.275	0.105	0.420	0.430	0.155
Bt1	33-67	0.366	0.097	0.490	0.500	0.134
Bt2	67-101	0.215	0.090	0.388	0.450	0.235
			Robinson Tract			
Ap	0-8	0.176	0.057	0.510	0.520	0.344
A	8-30	0.088	0.021	0.390	0.420	0.332
E1	30-42	0.124	0.034	0.491	0.501	0.376
E2	42-69	0.124	0.024	0.500	0.510	0.386
Bt1	69-107	0.276	0.134	0.334	0.380	0.104
			Bluff Field			
A	0-5	0.376	0.158	0.530	0.540	0.164
AB	5-20	0.368	0.190	0.450	0.460	0.092
Bt1	20-30	0.406	0.242	0.475	0.500	0.094
Bt2	30-56	0.406	0.192	0.494	0.568	0.162
Bt3	56-76	0.358	0.192	0.440	0.450	0.092
Bt4	76-102	0.401	0.204	0.490	0.500	0.099

† Effective Porosity: θ_s-θ_{fc}

Table 4. Regression coefficients and beta weights for the multiple linear equations fit to the data in this study. All regression equations are of the form $y=a+b_1(x_1)+b_2(x_2)\ldots+b_i(x_i)$.

Variable	Intercept	Midpoint Depth	Bulk Density	Silt	COLE†	Feret Diameter‡	Height‡	Width‡	Major Ellipse‡	Minor Ellipse‡	Relative Surface Area	Form Factor‡	R^2	MSE¶
		cm	g cm^{-3}	%		mm					mm^{-1}	mm^{-2}		
						Regression Coefficients								
Ksat	2960		-1900	-23.3								-1495§	0.609	0.018
θ_S	28.1		-14.2					-4.55	20.7§	12.5			0.697	0.007
Field Capacity (θ_{fc})	-4.8			0.222	141.3	10.05§							0.812	0.003
Permenant Wilting Point (θ_{pwp})	23.4				181.9	-16.4	15.6	20.5		-34.9			0.708	0.007
$\theta_{S\text{-}Index}$	44.8					-22.2§	24.4§				64.1		0.562	0.010
Effective Porosity (θ_S-θ_{fc})	40.6	-0.95		-0.255	-89.8								0.593	0.037
						Beta Weights								
Ksat			-0.553	-0.607								-0.264		
θ_S			-0.362					-0.844	0.568	0.997				
Field Capacity (θ_{fc})				0.393	0.540	0.255								
Permenant Wilting Point (θ_{pwp})					0.689	-2.487	1.933	2.901		-2.123				
θ S-Index						-0.617	0.754				0.623			
Effective Porosity (θ_S-θ_{fc})		-0.352		-0.461	-0.351									

† COLE, coefficient of linear extensibility.

‡ Average value for horizon used.

§ Indicates that the data used was first log normalized.

¶ MSE, Mean Standard Error

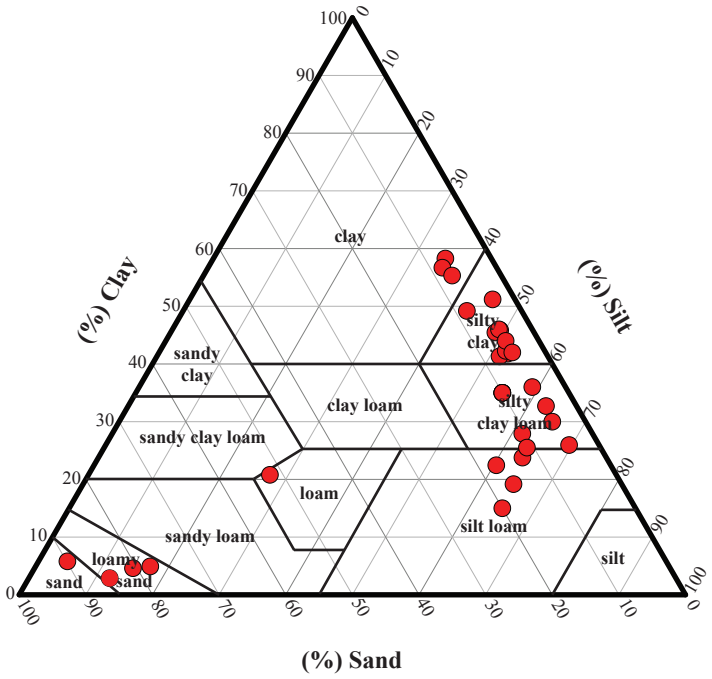

Fig. 1. Particle-size distribution of all samples used in this study.

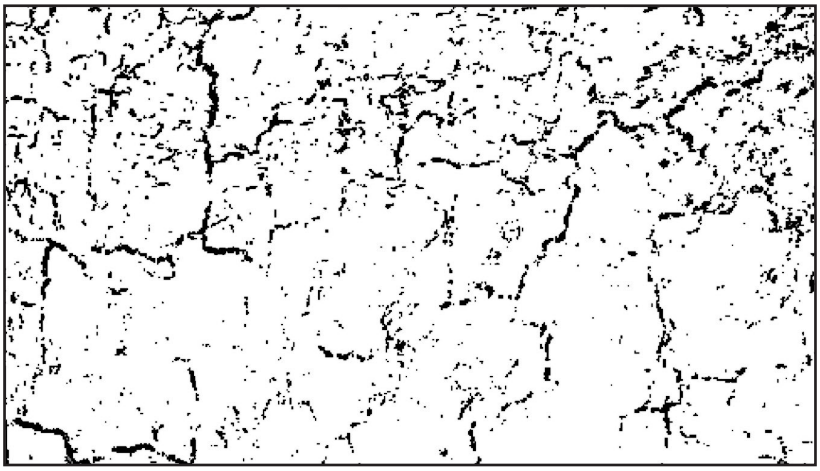

Fig. 2. Two-dimensional (2-D) image of Bt2 horizon from the Konza Agriculture field site. Three-dimensional surface scans were combined, cropped and projected on a 2-D plane for analyses in this work.

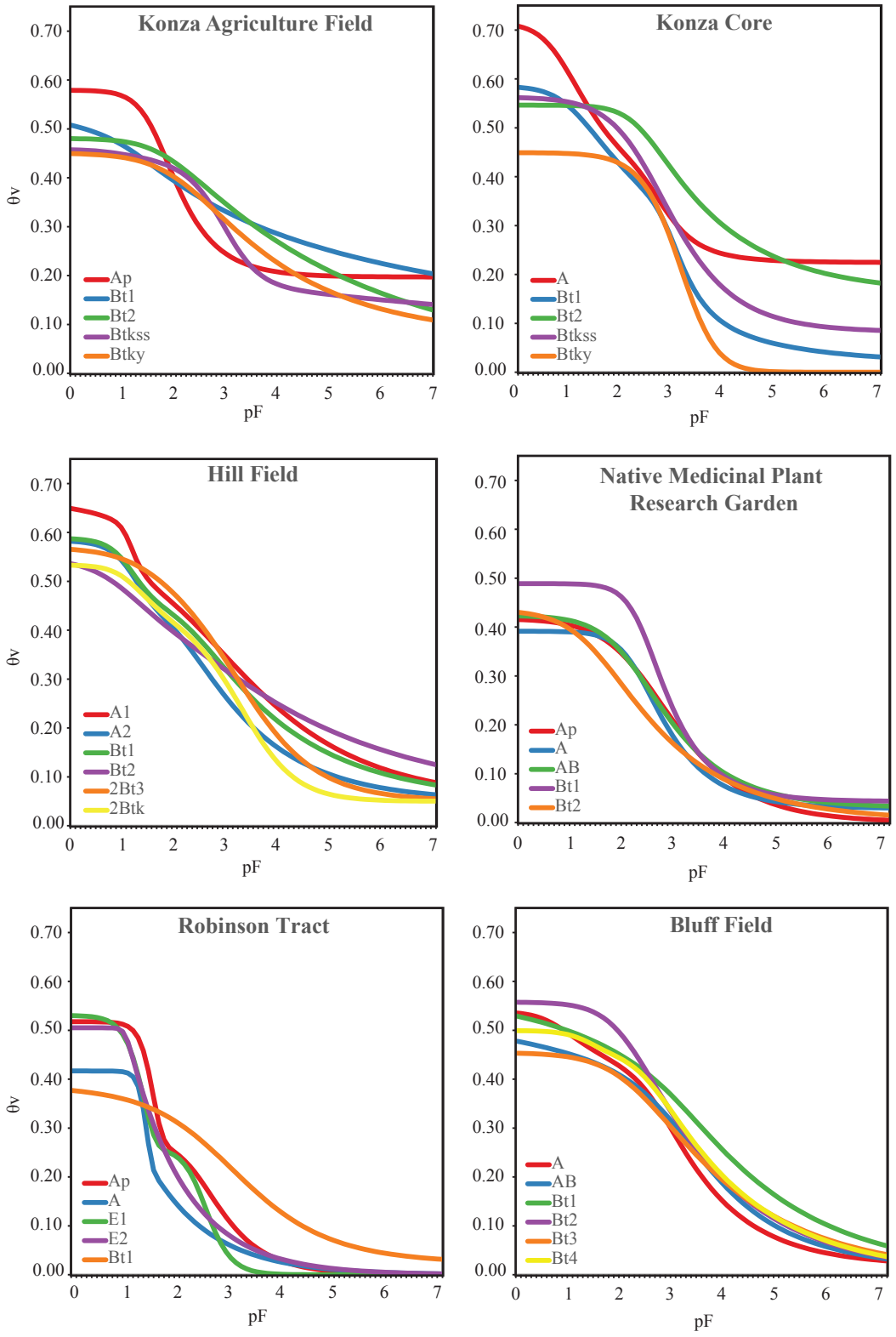

Fig. 3. Graphical representation of all water retention curves calculated for this study.

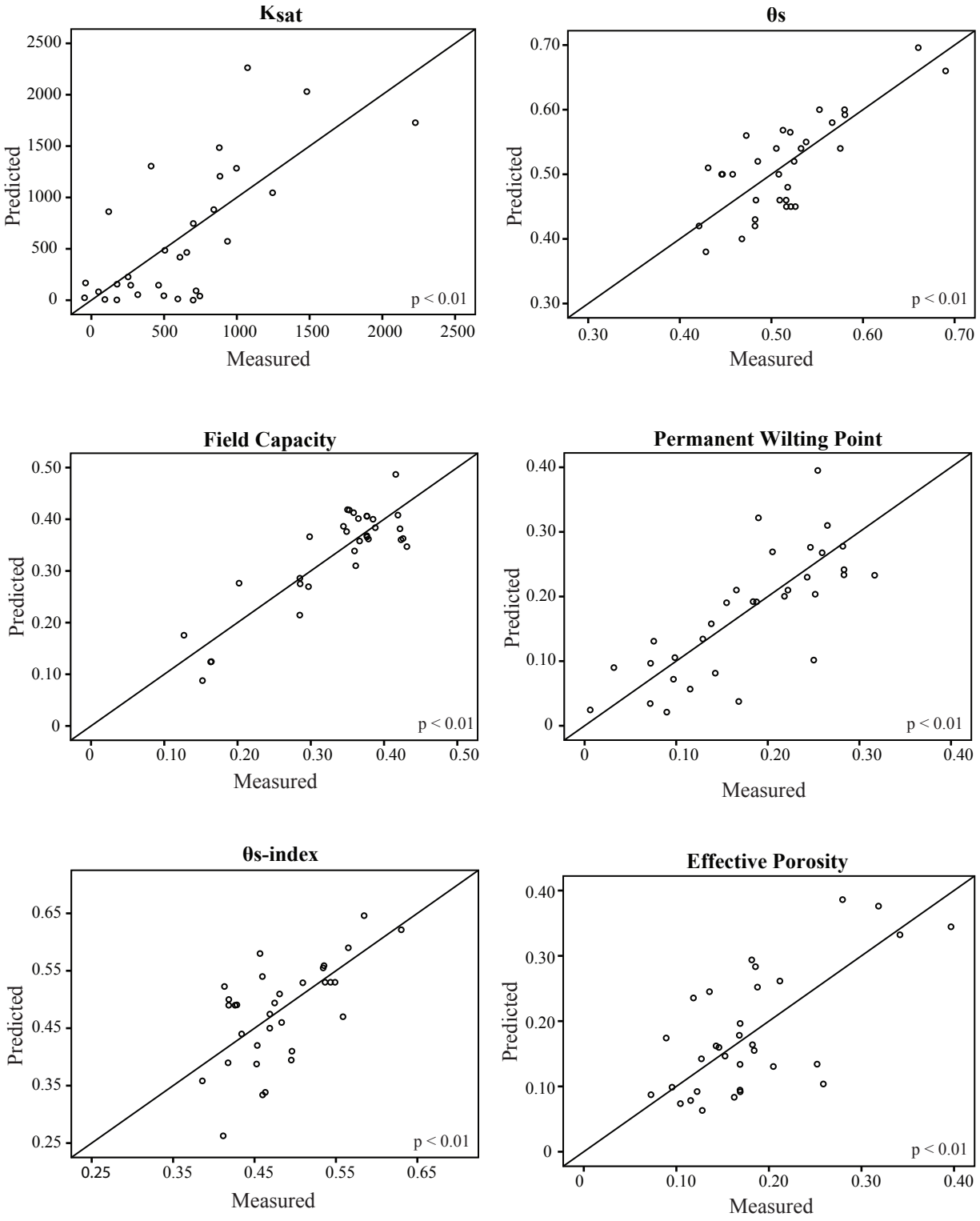

Fig. 4. Regression results compared to actual values for the water content at the S-index, permenant wilting point and water content at saturation. Many hydraulic properties were related to a combination of factors, primarily metrics derived from 3-D scanning of soil structure. See Table 3 for details.

CHAPTER 4. CONCLUSION

The use of meaningful quantitative metrics of soil structure proved useful for this study. Rather than relying on qualitative terms, these quantified metrics provided a solid basis from which soil structure can be compared directly to other properties. This work demonstrated the constraints to soil structure in multiple quantitative descriptions of size, relative fracture surface, abundance, and orientation. It also showed the possibilities for the development of pedotransfer functions using soil structural data to predict soil hydraulic properties. While additional research is required to verify these findings on a broader scale, these results may have important implications to understanding the genesis of soil structure and hydraulic properties.

APPENDIX A. COMPUTER CODE USED TO CREATE BAGPLOTS USING R FOR STATISTICAL COMPUTING

The following script was used to create the bagplots used in Chapter 2 of this thesis. R version 3.2.0 was used in computation.

```
#Packages needed to run script


library(car)
library(lattice)
library(aplpack)


#Read in data already formatted in csv file

data <- read.csv('data.csv')
half <- read.csv('shortstuff.csv')
sclay <- read.csv('shortclay.csv')

#Visual check of data

View(data)
View(half)
View(sclay)


#Set each variable used

midpoint <- data$midpoint
sand <- data$lnsand
clay <- data$clay
oc <- data$lnoc
cole <-data$cole
fclay<-data$fclay
clayoc<-data$clayoc

ssmidpoint <- half$midpoint

sclclay <- sclay$clay
sclrelsur <- sclay$relsurfarea

################################
pdf(file="abundance.pdf",height=11,width=8.5)
par(mfrow=c(2,2),omi=c(1,1,1,1))
```

```
bagplot(fclay,data$poredensity,xlab="fclay",ylab="pore density",
factor=3,show.whiskers=FALSE, show.bagpoints=TRUE)

bagplot(sand,data$poredensity,xlab="sand",ylab="pore density",
factor=3,show.whiskers=FALSE, show.bagpoints=TRUE)

dev.off()

################################

pdf(file="relative_fracture_surface.pdf",height=11,width=8.5)
par(mfrow=c(2,2),omi=c(1,1,1,1))

bagplot(oc,data$relsurfarea,xlab="oc",ylab="Relative Surface Area",
factor=3,show.whiskers=FALSE, show.bagpoints=TRUE)

bagplot(sclclay,sclrelsur,xlab="clay b horiz",ylab="Relative Surface Area",
factor=3,show.whiskers=FALSE, show.bagpoints=TRUE)

bagplot(sand,data$relsurfarea,xlab="sand",ylab="Relative Surface Area",
factor=3,show.whiskers=FALSE, cex=0, show.bagpoints=TRUE)

bagplot(clay,data$relsurfarea,xlab="clay",ylab="Relative Surface Area",
factor=3,show.whiskers=FALSE, show.bagpoints=TRUE)

dev.off()

################################

pdf(file="Size.pdf",height=11,width=8.5)
par(mfrow=c(2,2),omi=c(1,1,1,1))

bagplot(fclay,data$logminferet,xlab="fclay",ylab="log(minimum feret)",
factor=3,show.whiskers=FALSE, show.bagplots=TRUE)

bagplot(clay,data$logmincole,xlab="clay/oc",ylab="log(minimum feret)",
factor=3,show.whiskers=FALSE, show.bagpoints=TRUE)

bagplot(clay,data$logminferet,xlab="clay",ylab="log(minimum feret)",
factor=3,show.whiskers=FALSE, show.bagpoints=TRUE)

bagplot(sand,data$logminferet,xlab="sand",ylab="log(minimum feret)",
factor=3,show.whiskers=FALSE, show.bagpoints=TRUE)

bagplot(clay,data$logavgferetdi,xlab="clay",ylab="log(feret diameter)",
factor=3,show.whiskers=FALSE, show.bagpoints=TRUE)
```

```
bagplot(clay,data$fercole,xlab="clay",ylab="log(feret diameter)/COLE",
factor=3,show.whiskers=FALSE, show.bagpoints=TRUE)

bagplot(sand,data$logavgferetdi,xlab="sand",ylab="log(feret diameter)",
factor=3,show.whiskers=FALSE, show.bagpoints=TRUE)

dev.off()

###################################

pdf(file="orientation.pdf",height=11,width=8.5)
par(mfrow=c(2,2),omi=c(1,1,1,1))

bagplot(midpoint,data$avgelipang,xlab="midpoint",ylab="ellipse angle",
factor=3,show.whiskers=FALSE, show.bagpoints=TRUE)

bagplot(ssmidpoint,sselipang,xlab="midpoint",ylab="ellipse angle",
factor=3,show.whiskers=FALSE, show.bagpoints=TRUE)

bagplot(fclay,data$avgelipang,xlab="fclay",ylab="ellipse angle",
factor=3,show.whiskers=FALSE, show.bagpoints=TRUE)

dev.off()
```

APPENDIX B. USING EXCEL SOLVER FUNCTION TO ESTIMATE THE DURNER PARAMETERS FOR WATER RETENTION FROM MEASURED POTENTIAL AND WATER CONTENT VALUES

The equation for effective saturation is:

$$S_e = \frac{\theta_\varphi - \theta_r}{\theta_s - \theta_r} \quad [1]$$

Where, S_e is the effective saturation,

θ_r is the residual volumetric water content,

θ_s is the saturated volumetric water content, and

θ_φ is the volumetric water content θ at any given potential head φ in cm.

It is written in the Durner (1994) model as:

$$S_e = w_1 \left[\frac{1}{1 + (\alpha_1|\varphi|)^{n_1}}\right]^{m_1} + w_2 \left[\frac{1}{1 + (\alpha_2|\varphi|)^{n_2}}\right]^{m_2} \quad [2]$$

Where $|\varphi|$ is the measured potential head (measured in cm)

This can be rewritten in terms of θ_φ

$$\theta_\varphi = \theta_r + w_1 \left[\frac{\theta_s - \theta_r}{((1 + \alpha_1|\varphi|)^{n_1})^{m_1}}\right] + w_2 \left[\frac{\theta_s - \theta_r}{((1 + \alpha_2|\varphi|)^{n_2})^{m_2}}\right] \quad [3]$$

Where θ_φ is the calculated water content θ at any given potential φ; $\theta_r$is the calculated residual moisture content, and θ_s is the measured volumetric water content at saturation, derived from the phi value:

$$\frac{1}{\rho_b} \quad [4]$$

Where ρ_b is the measured bulk density of the soil for a given sample.

To solve the equation in Microsoft Excel (2013) the minimum value for the following equation was calculated in *solver:*

$$\sum_{i=1}^{n} \Delta\theta \quad [5]$$

$$\Delta\theta = \left(\theta_{\varphi_m} - \theta_{\varphi}\right) * 1000 \quad [6]$$

Where θ_{φ} is the calculated θ at any given potential; θ_{φ_m} is the measured θ at the same given potential and n is the number of measured θ samples for a given horizon.

Goodness of fit was calculated by correlating measured θ values to calculated ones using Pearson product-moment coefficient, using the RSQ function in Excel.

In the solver dialog box, the following constraints were used:

$\theta_r > 0$	$\alpha_2 > 0$	$n_2 > 0$	$m_2 > 0$
$\theta_r < 5$	$n_1 > 0$	$n_2 < 2$	$w_1 > 0$
$\alpha_1 > 0$	$n_1 < 2$	$m_1 > 0$	$w_2 > 0$

This least square fitting method was adapted from a similar method developed for the van Genuchten water retention curve (van Genuchten, 1980) by Ruediger Anlauf, Ph.D, Professor of Physics of Soils and Growing Media at Osnabrueck University of Applied Sciences. (2014)

REFERENCES

Anlauf, R. 2014. Using the EXCEL solver function to estimate the van Genuchten parameters from measured pF/water content values. Excel spreadsheet retrieved from www.al.hs-osnabrueck.de/anlauf.html on [6/7/2015].

Durner, W. 1994. Hydraulic conductivity estimation for soils with heterogeneous pore structure. Water Resource Research. 30:211-223.

van Genuchten, M.Th. 1980. A closed-form equation for predicting the hydraulic conductivity of unsaturated soils. Soil Science Society of America Journal. 44:892-898.

APPENDIX C. USING EXCEL SOLVER FUNCTION TO CALCULATE THE S-INDEX FROM DURNER PARAMETERS FOR WATER RETENTION

The S-index of a water retention curve is the slope of the inflection point along the structural pores of a bimodal water retention curve (i.e. Durner, 1994). The S-index has been used as a measure of soil physical condition (Dexter, 2004) which is impacted by soil structure. Additionally, the water content at the inflection point (θ_i) has been identified as the optimum water content for tillage (Dexter and Bird 2001).

The equation to solve for the S-index is:

$$S(h) = \frac{\alpha^n (\theta_s - \theta_r) mn(-h)^{n-1}}{[1 + (-\alpha h)^n]^{m+1}} \quad [1]$$

Where S is the S-index,

α is the alpha of the structural domain of the water retention curve,

θ_s is the saturated volumetric water content,

θ_r is the residual volumetric water content of the water retention curve,

m is the m-value of the structural domain of the water retention curve,

n is the n-value of the structural domain, and

h is the water head (in cm)

The S-index is the second derivative of the water retention curve, so the value of this index is the maximum value. To solve for this value in Microsoft Excel (2013), the maximum value for *h* [eq. 1] was solved for using *solver*.

In the solver dialog box, the following constraint was used:

$$\theta_i < \theta_s \quad [2]$$

REFERENCES

Dexter, A.R. 2004. Soil physical quality part I. Theory, effects of soil texture, density, and organic matter, and effects on root growth. Geoderma. 120:201-214.

Dexter, A.R and N.R.A. Bird. 2001. Methods for predicting the optimum and the range of soil water contents for tillage based on the water retention curve. Soil and Tillage Research. 57:203-212.

Durner, W. 1994. Hydraulic conductivity estimation for soils with heterogeneous pore structure. Water Resource Research. 30:211-223.